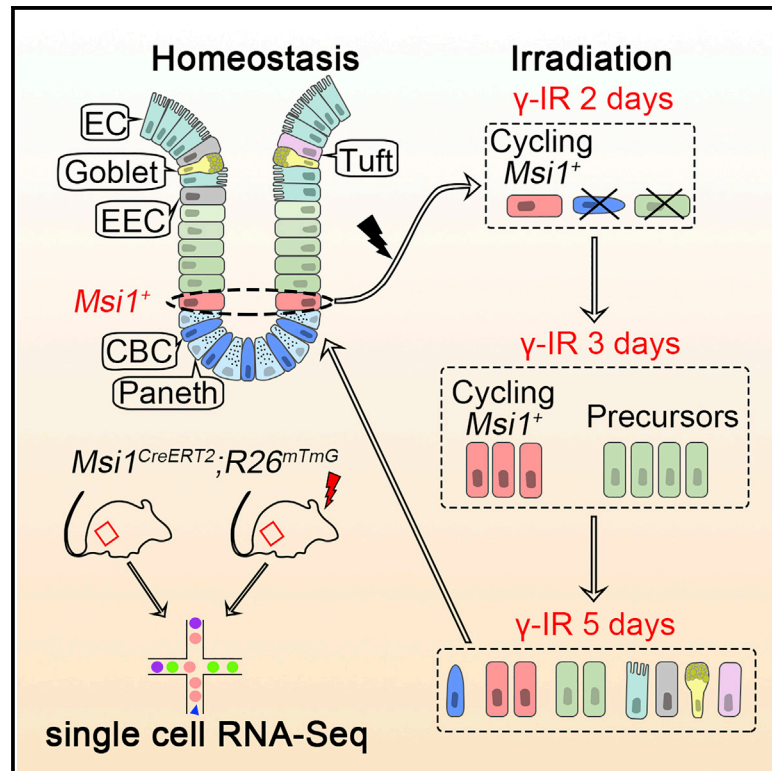


# Cycling Stem Cells Are Radioresistant and Regenerate the Intestine

## Graphical Abstract



## Authors

Xiaole Sheng, Ziguang Lin, Cong Lv, ..., Bogi Andersen, Fazheng Ren, Zhengquan Yu

## Correspondence

renfazheng@cau.edu.cn (F.R.), zyu@cau.edu.cn (Z.Y.)

## In Brief

Quiescent reserve stem cells in the intestine are thought to activate following irradiation to restore the depleted *Lgr5*<sup>high</sup> CBCs. Now, Sheng et al. demonstrate that cycling *Msi1*<sup>+</sup> cells represent DNA damage-resistant ISCs that support efficient repopulation of the intestinal epithelium at the early stage of post-radiation repair, ahead of *Lgr5*<sup>high</sup> CBCs.

## Highlights

- Cycling *Msi1*<sup>+</sup> ISCs in the intestinal crypt are DNA damage resistant
- *Msi1*<sup>+</sup> ISCs enable fast intestinal repair ahead of *Lgr5*<sup>high</sup> CBCs
- Paneth cells preferentially arise from *Msi1*<sup>+</sup> ISCs during homeostasis and repair



## Article

# Cycling Stem Cells Are Radioresistant and Regenerate the Intestine

Xiaole Sheng,<sup>1,13</sup> Ziguang Lin,<sup>2,13</sup> Cong Lv,<sup>1,13</sup> Chunlei Shao,<sup>1</sup> Xueyun Bi,<sup>1</sup> Min Deng,<sup>1</sup> Jiuzhi Xu,<sup>1</sup> Christian F. Guerrero-Juarez,<sup>3,4</sup> Mengzhen Li,<sup>1</sup> Xi Wu,<sup>1</sup> Ran Zhao,<sup>1</sup> Xu Yang,<sup>1</sup> Guilin Li,<sup>1</sup> Xiaowei Liu,<sup>5</sup> Qingyu Wang,<sup>6</sup> Qing Nie,<sup>3</sup> Wei Cui,<sup>7</sup> Shan Gao,<sup>8</sup> Hongquan Zhang,<sup>9</sup> Zhihua Liu,<sup>10</sup> Yingzi Cong,<sup>11</sup> Maksim V. Plikus,<sup>4</sup> Christopher J. Lengner,<sup>12</sup> Bogi Andersen,<sup>2</sup> Fazheng Ren,<sup>6,\*</sup> and Zhengquan Yu<sup>1,14,\*</sup>

<sup>1</sup>Key Laboratory of Precision Nutrition and Food Quality, Ministry of Education, Department of Nutrition and Health, College of Biological Sciences, China Agricultural University, Beijing 100193, China

<sup>2</sup>Departments of Medicine and Biological Chemistry, University of California, Irvine School of Medicine, Irvine, CA 92697, USA

<sup>3</sup>Department of Mathematics, NSF-Simons Center for Multiscale Cell Fate Research, University of California, Irvine, Irvine, CA 92697, USA

<sup>4</sup>Department of Developmental and Cell Biology, Sue and Bill Gross Stem Cell Research, Center for Complex Biological Systems, University of California, Irvine, Irvine, CA 92697, USA

<sup>5</sup>Department of Gastroenterology, Xiangya Hospital of Central South University, Changsha 410008, Hunan, China

<sup>6</sup>Beijing Advanced Innovation Center for Food Nutrition and Human Health, China Agricultural University, Beijing, China

<sup>7</sup>Institute of Reproductive and Developmental Biology, Faculty of Medicine, Imperial College London, London, UK

<sup>8</sup>CAS Key Laboratory of Bio-medical Diagnostics, Suzhou Institute of Biomedical Engineering and Technology, Chinese Academy of Sciences, Suzhou, Jiangsu 215163, China

<sup>9</sup>Laboratory of Molecular Cell Biology and Tumor Biology, Department of Anatomy, Histology and Embryology, Beijing 100191, China

<sup>10</sup>State Key Laboratory of Molecular Oncology, National Cancer Center/Cancer Hospital, Chinese Academy of Medical Sciences, Beijing 100021, China

<sup>11</sup>Department of Microbiology and Immunology, University of Texas Medical Branch, Galveston, TX, USA

<sup>12</sup>Department of Biomedical Sciences, School of Veterinary Medicine, and Institute for Regenerative Medicine, University of Pennsylvania, Philadelphia, PA, USA

<sup>13</sup>These authors contributed equally

<sup>14</sup>Lead Contact

\*Correspondence: [renfazheng@cau.edu.cn](mailto:renfazheng@cau.edu.cn) (F.R.), [zyu@cau.edu.cn](mailto:zyu@cau.edu.cn) (Z.Y.)  
<https://doi.org/10.1016/j.celrep.2020.107952>

## SUMMARY

A certain number of epithelial cells in intestinal crypts are DNA damage resistant and contribute to regeneration. However, the cellular mechanism underlying intestinal regeneration remains unclear. Using lineage tracing, we show that cells marked by an *Msi1* reporter (*Msi1*<sup>+</sup>) are right above *Lgr5*<sup>high</sup> cells in intestinal crypts and exhibit DNA damage resistance. Single-cell RNA sequencing reveals that the *Msi1*<sup>+</sup> cells are heterogeneous with the majority being intestinal stem cells (ISCs). The DNA damage-resistant subpopulation of *Msi1*<sup>+</sup> cells is characterized by low-to-negative *Lgr5* expression and is more rapidly cycling than *Lgr5*<sup>high</sup> radiosensitive crypt base columnar stem cells (CBCs). This enables an efficient repopulation of the intestinal epithelium at early stage when *Lgr5*<sup>high</sup> cells are not emerging. Furthermore, relative to CBCs, *Msi1*<sup>+</sup> cells preferentially produce Paneth cells during homeostasis and upon radiation repair. Together, we demonstrate that the DNA damage-resistant *Msi1*<sup>+</sup> cells are cycling ISCs that maintain and regenerate the intestinal epithelium.

## INTRODUCTION

The intestinal epithelium is a single-layer tissue organized into repetitive crypt-villus units. The cells that drive homeostatic intestinal renewal reside at the bottom of the crypt and move upward toward the villus tip, where they eventually die—a process referred to as the conveyor-belt model (Heath, 1996). The intestinal epithelium undergoes rapid turnover, with the majority of epithelial cells replaced in 3 to 5 days in mice (Heath, 1996). The rapid turnover of intestinal epithelial cells renders them sensitive to irradiation. Consequently, patients undergoing radiation therapy to the abdomen, pelvis, or rectum develop acute enter-

itis, displaying symptoms that include pain, bloating, nausea, fecal urgency, diarrhea, and rectal bleeding (Stacey and Green, 2014). Mucosal healing is critical for the remission of DNA damage-induced enteritis. Therefore, elucidating the cellular mechanisms of mucosal healing is necessary to develop new therapies for post-radiation enteritis.

Intestinal stem cells (ISCs), which reside within the proliferative compartment of crypts, are responsible for both intestinal homeostasis and epithelial regeneration after radiation exposure (Barker, 2014; Li and Clevers, 2010). Multiple studies have shown the existence of two functionally distinct ISC populations (Barker, 2014; Gehart and Clevers, 2015; Li and Clevers, 2010): mitotically



active *Lgr5<sup>high</sup>* ISCs, commonly known as crypt base columnar stem cells, or CBCs (Barker et al., 2007; Sato et al., 2009), and more dormant, reserve ISCs, defined as +4 cells due to their location within crypts (Li et al., 2014; Montgomery et al., 2011; Powell et al., 2012; Sangiorgi and Capecchi, 2008; Takeda et al., 2011; Tian et al., 2011). Although CBCs mainly function to maintain physiological homeostasis of intestinal epithelium (Barker et al., 2007; Sato et al., 2009), they are also thought to be indispensable for epithelial regeneration (Metcalfe et al., 2014). *In vitro*, a single *Lgr5<sup>high</sup>* CBC can form a mini-gut structure that contains all mature intestinal cell types (Sato et al., 2009). Therefore, CBCs have been proposed to be bona fide ISCs. In contrast, considerable controversy exists regarding the precise identity of +4 cells and their lineage relationship to CBCs. It remains unclear whether +4 cells are bona fide ISCs. Several markers of +4 cells, including *Bmi1*, *mTert*, and *Hopx*, have been identified by *in vivo* lineage tracing, either by knockin of CreER into the gene or by randomly integrated transgenesis (Barker, 2014; Montgomery et al., 2011; Sangiorgi and Capecchi, 2008; Takeda et al., 2011; Tian et al., 2011). In contrast to CBCs, +4 cells are resistant to DNA damage and are activated to promote epithelial regeneration upon radiation-induced CBC depletion. In addition to +4 cells, progenitors of secretory and absorptive cells also contribute to the regeneration of damaged intestinal epithelium at relatively low efficiency (Buczacki et al., 2013; Tetteh et al., 2016; van Es et al., 2012; Yu et al., 2018). Importantly, +4 cells are thought to be reserve ISCs, and their cell-cycle quiescence has been proposed to be the main source of their radioresistance. The primary evidence for +4 cells' quiescence is that the +4 position corresponds to label retaining cells (Potten et al., 1974, 2002), and +4 cells expressing *Bmi1*, *Hopx*, and *mTert* undergo slower kinetics of lineage tracing in comparison to *Lgr5*-expressing ISCs (Montgomery et al., 2011; Powell et al., 2012; Takeda et al., 2011; Yan et al., 2012). Further evidence is that *Hopx<sup>CreER</sup>* cells were shown to reside in G0 (Li et al., 2016). However, three independent studies have demonstrated that label-retaining cells are, in fact, terminally differentiated Paneth cells or secretory progenitors (Buczacki et al., 2013; Li et al., 2016; Steinhäuser et al., 2012). Additionally, it is worth mentioning that the primary DNA damage repair pathway in quiescent stem cells is non-homologous end joining (NHEJ), which is nonspecifically activated at all cell-cycle stages, and that it is error prone and unfavorable for tissue repair (Mohrin et al., 2010). In comparison, homologous recombination (HR)-mediated acute DNA repair can only occur in cycling cells during late S and G2 phases (Maity et al., 1994; Moynahan and Jasin, 2010; Shaltiel et al., 2015). Therefore, the identity of +4 cells and the mechanisms underlying +4 cell-mediated epithelial regeneration remain uncertain.

Here, we generated an *Msi1<sup>CreERT2</sup>* allele for lineage tracing and observe that *Msi1<sup>CreERT2</sup>*-marked cells are enriched at the +4 position in intestinal crypt, referred to as *Msi1<sup>+</sup>* cells, and are resistant to DNA damage. Single-cell RNA sequencing (scRNA-seq) of *Msi1<sup>+</sup>* cells further revealed that a subset of S/G2-phase stem cells, characterized by low-to-negative *Lgr5* expression, exhibit DNA-damage resistance and repopulate radiation-damaged epithelium at early stage when *Lgr5<sup>high</sup>* cells are not emerging, which substantially differs from the classic theory that such +4 cells function as reserve stem cells, activate

following irradiation to restore the depleted *Lgr5<sup>high</sup>* CBCs first, and then nascent CBCs rapidly divide to repair damaged intestinal epithelium. Furthermore, we observed that *Msi1<sup>+</sup>* cells preferentially produce the Paneth lineage, relative to CBCs.

## RESULTS

### An *Msi1* Reporter Is Enriched for DNA Damage-Resistant ISCs

*Msi1* has been identified as a marker for ISCs, including both CBCs and +4 cells (Kayahara et al., 2003; Li et al., 2015). We first validated *Msi1* expression pattern in CBCs and +4 cells at the protein level using immunohistochemistry (Figure S1A). At the RNA level, *Msi1* expression was the strongest in +4 cells (Figure S1B). To track the fate of *Msi1*-expressing cells within intestinal epithelium, we generated a tamoxifen (TAM)-inducible Cre (*CreERT2*) knockin targeted just before the stop codon of the endogenous *Msi1* locus (Figure S1C). We then crossed *Msi1<sup>CreERT2</sup>* mice with *R26<sup>Lox-Stop-Lox-LacZ</sup>* (*R26R<sup>LacZ</sup>*) reporter mice. Fifteen hours after one pulse of TAM, X-gal staining showed that 15.7% of intestinal crypts were labeled, and *Msi1* reporter-marked cells were mainly located at the +4 position of intestinal crypts (Figures 1A and 1B), which were further corroborated in *Msi1<sup>CreERT2</sup>;R26<sup>mTmG</sup>* mice (Figure 1C). Thus, *Msi1<sup>CreERT2</sup>*-marked cells are largely positionally distinct from *Lgr5<sup>high</sup>* CBCs (Figures 1A and 1B).

2 days after TAM induction, most labeled crypts contained 3–7 cells exhibiting  $\beta$ -galactosidase activity (Figure 1D). One week after induction, X-gal staining became more widespread (Figures 1D and S1D), and the labeling cells included differentiated cell lineages—Paneth, goblet, and enteroendocrine cells (EECs) (Figure 1E). The number of fully labeled crypt-villus ribbons and the percentage of LacZ<sup>+</sup> crypts sustained over time (Figures 1D and S1E), and *Msi1* reporter marked progeny existed for at least 1 year (Figure 1D). Next, we sought to examine how *Msi1* reporter-marked cells give rise to distinct cell lineages. We quantified the positions of labeled cells 1 day after TAM induction, a time point when newly generated cells are emerging, and found that the majority of labeled cells move both upward and downward relative to +4 positions (Figure 1F). This distribution suggests that *Msi1* reporter-marked cells concomitantly give rise to distinct lineages, including CBCs, Paneth cells, and villus cells. The expression of CBC markers and Wnt target genes (*Lgr5*, *Axin2*, *Sox9*, and *Olfm4*) in *Msi1<sup>CreERT2</sup>*-marked cells was similar to that of cells marked with *Hopx<sup>CreERT2</sup>*, a well-established marker of +4 ISCs (Takeda et al., 2011), and distinct from that of *Lgr5<sup>high</sup>* CBCs (Figures S1F and S1G). Collectively, these data demonstrate that *Msi1* reporter-marked cells are primarily located above the crypt base and the CBC compartment and exhibit multipotent stem cell properties.

To examine the DNA damage response by *Msi1<sup>+</sup>* cells, we exposed *Msi1<sup>CreERT2</sup>;R26R<sup>LacZ</sup>* and *Lgr5<sup>EGFP-IRES-CreERT2</sup>;R26R<sup>LacZ</sup>* mice to 12 Gy of ionizing radiation ( $\gamma$ -IR), 15 h after a single pulse of TAM. After  $\gamma$ -IR exposure, the number of LacZ<sup>+</sup> ribbons produced by *Msi1<sup>+</sup>* cells was similar to what we observed during homeostasis, whereas the number of LacZ<sup>+</sup> ribbons from *Lgr5* reporter-marked cells was strongly reduced (Figure 1G). Lineage-tracing analysis in *Msi1<sup>CreERT2</sup>;R26<sup>mTmG</sup>* mice also



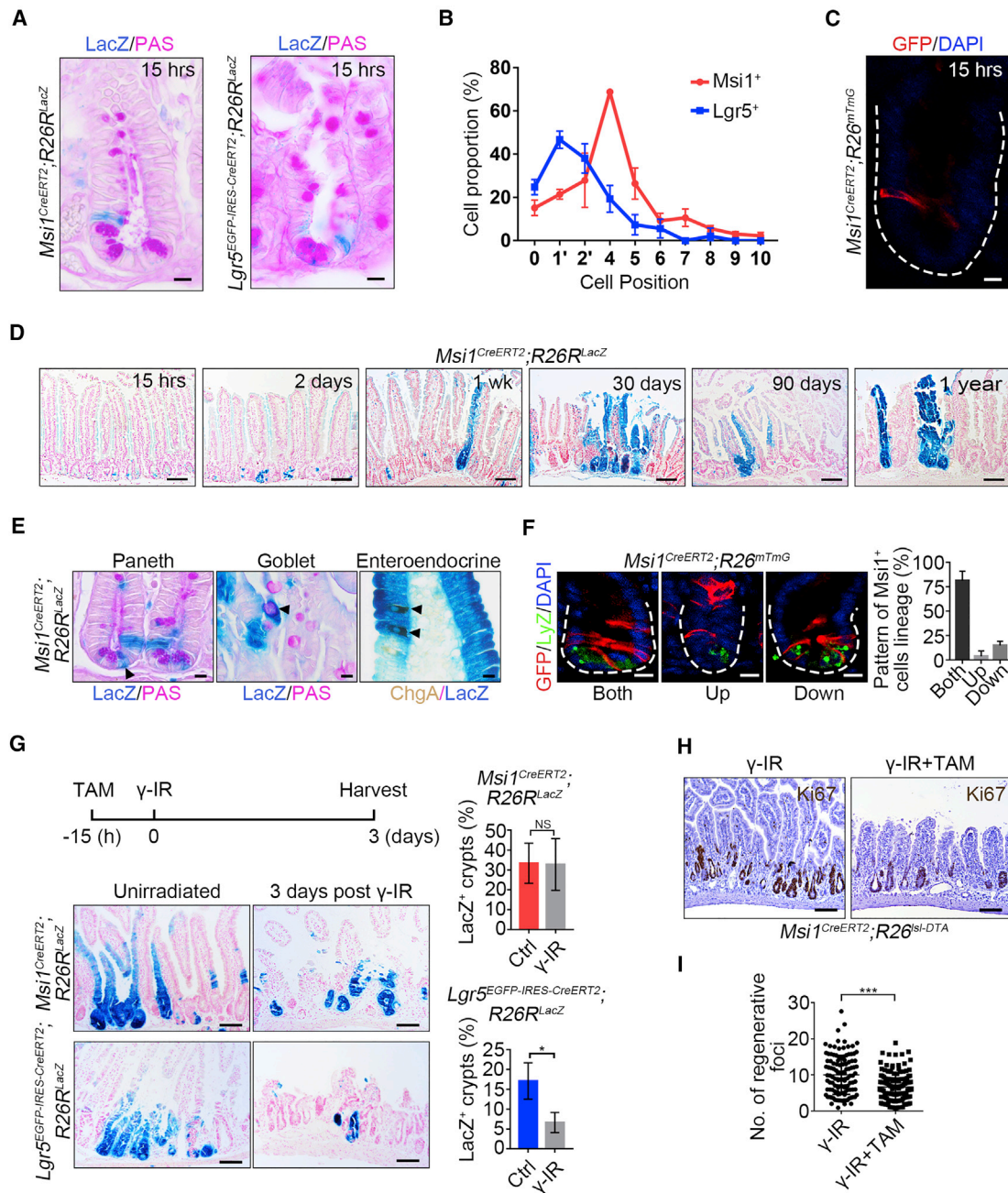


**Figure 1. *Msi1* Reporter-Marked Cells Are Enriched at +4 Position in Intestinal Crypts**

(A) Representative images of LacZ<sup>+</sup> cells in *Msi1*<sup>CreERT2</sup>;*R26R*<sup>LacZ</sup> (302 crypts; n = 3 mice) and *Lgr5*<sup>EGFP-IRES-CreERT2</sup>;*R26R*<sup>LacZ</sup> (175 crypts; n = 3 mice) lineage-labeled small intestinal crypts 15 h after TAM induction. Scale bar, 10 μm.

(B) Quantification of the position of LacZ<sup>+</sup> cells in intestinal crypts in (A). Data represent the mean value ± SD.

(C) Representative images of GFP<sup>+</sup> cells in *Msi1*<sup>CreERT2</sup>;*R26*<sup>mTmG</sup> lineage-labeled small intestinal crypts 15 h after TAM induction. n = 3 mice. Scale bar, 10 μm.

(D) Low-magnification images of the LacZ<sup>+</sup> ribbon in *Msi1*<sup>CreERT2</sup>;*R26R*<sup>LacZ</sup> lineage-labeled small intestine at different time points following TAM induction. n ≥ 3 mice at each time point. Scale bar, 40 μm.

(E) Periodic acid-Schiff (PAS) staining and immunohistochemistry for ChgA in *Msi1*<sup>CreERT2</sup>;*R26R*<sup>LacZ</sup> lineage-labeled small intestine 1 week after TAM induction. n = 3 mice. Scale bar, 10 μm.

(F) Double immunofluorescence for GFP and lysozyme in *Msi1*<sup>CreERT2</sup>;*R26*<sup>mTmG</sup> lineage-labeled small intestinal crypts one day after TAM induction. The position of GFP<sup>+</sup> cells is above the +4 position, referred to as “Up”; below the +4 position, referred to as “Down”; above and below the +4 position, referred to as “Both.” Quantification of the lineage pattern of *Msi1*-reporter<sup>+</sup> cells (n = 91 crypts; n = 3 mice). Data represent the mean value ± SD. Scale bar, 10 μm.

(G) Representative images of LacZ<sup>+</sup> ribbons in *Msi1*<sup>CreERT2</sup>;*R26R*<sup>LacZ</sup> (Ctrl-720 crypts, n = 3 mice; γ-IR-540 crypts, n = 4 mice) and *Lgr5*<sup>EGFP-IRES-CreERT2</sup>;*R26R*<sup>LacZ</sup> (Ctrl-808 crypts, n = 3 mice; γ-IR-852 crypts, n = 4 mice) lineage-labeled small intestines 4 days after TAM induction, or the mice were irradiated after 15 h of TAM

(legend continued on next page)

demonstrated a robust repopulating capacity of *Msi1*<sup>+</sup> cells after exposure to  $\gamma$ -IR (Figure S1H). In order to rule out the interference of TAM remains, we isolated intestinal organoids of *Msi1*<sup>CreERT2</sup>;*R26*<sup>mTmG</sup> mice. The organoids were incubated with 4-hydroxytamoxifen (4-OH) for 9.5 h then replaced with 4-OH-free medium to make sure only the initial *Msi1*<sup>+</sup> cells were labeled. Quantification of the position showed that the initial labeled *Msi1*<sup>+</sup> cells were also enriched at +4 position (Figure S1I), similar to its pattern *in vivo*. Then, we exposed the labeled organoids from *Msi1*<sup>CreERT2</sup>;*R26*<sup>mTmG</sup> and *Lgr5*<sup>EGFP-IRES-CreERT2</sup>;*R26*<sup>sl-tdT</sup> mice to 6 Gy  $\gamma$ -IR to examine the regeneration ability of *Msi1*<sup>+</sup> versus *Lgr5*<sup>+</sup> cells. Six days after  $\gamma$ -IR, the number of traced organoids produced by *Msi1*<sup>+</sup> cells was similar to that under control conditions, while the number of traced organoids from *Lgr5*<sup>+</sup> cells was significantly reduced (Figures S2A–S2D). Those findings indicate that *Msi1*<sup>+</sup> cells are radioresistant, able to survive  $\gamma$ -IR, and repopulate the damaged epithelium.

Furthermore, we used *Msi1*<sup>CreERT2</sup>;*R26*<sup>sl-DTA</sup> mice to examine the importance of *Msi1*<sup>+</sup> cells during intestine damage regeneration. Twenty-four hours after a single pulse of TAM injection, apparent apoptosis was detected at the base of crypts (Figure S2E). We found that the depletion of *Msi1*<sup>+</sup> cells significantly impaired intestinal epithelial regeneration following  $\gamma$ -IR (Figures 1H and 1I). Similarly, using *Msi1*<sup>CreERT2</sup>;*R26*<sup>mTmG</sup>;*R26*<sup>sl-DTR</sup> mouse model, the depletion of *Msi1* reporter<sup>+</sup> cells is more efficient, and the impairment of intestinal regeneration becomes more obvious (Figures S2F–S2H). Taken together, these findings suggest that *Msi1*<sup>+</sup> cells are DNA damage-resistant ISCs with the capacity to repopulate  $\gamma$ -IR-damaged epithelium.

### *Msi1*<sup>+</sup> Cells Are a Heterogeneous Population

Next, we sought to better characterize the identity of *Msi1*<sup>+</sup> cells using scRNA-seq analysis. GFP-labeled cells from *Msi1*<sup>CreERT2</sup>;*R26*<sup>mTmG</sup> mice were sorted 15 h after TAM induction, and subjected to scRNA-seq (Figure S3A; Table S1). Unsupervised clustering (Duò et al., 2018) identified nine distinct cell clusters (Figure 2A). We utilized the differentially expressed gene signatures to assign putative cell type identities to these clusters (Figures 2B–2D, S3B, and S3C). Cluster H15h-C1 (at homeostasis, traced for 15 h) is enriched in cells expressing the highest levels of ISC marker gene *Lgr5*, as well as several other ISC marker genes, namely, *Gkn3*, *Ascl2*, *Olfm4*, *Jun*, *Pdgfra*, and *2210407c18Rik* (Figures 2C and S3C). Thus, H15h-C1 cells were defined as *Lgr5*<sup>high</sup> ISCs. Clusters of H15h-C2 and H15h-C3 cells have low or negative *Lgr5* status, but concomitantly express the ISC marker genes *Igfbp4* and *Ascl2* (Figure 2C), on which basis they are classified as *Lgr5*<sup>low/neg</sup> ISCs. In comparison to H15h-C2 cells, H15h-C3 cells highly express G2/M-phase marker genes (Figure 2D). Consistently, single-cell consensus clustering

(SC3) analysis (Kiselev et al., 2017) of clusters H15h-C1, H15h-C2, and H15h-C3 revealed higher similarity between H15h-C2 and H15h-C3 cells, relative to H15h-C1 ISCs, and further divided H15h-C1 cells into two sub-clusters (Figure 2E). Cluster H15h-C4 cells are also enriched for G2/M-phase marker genes (Figure 2D), and principal component analysis (PCA) analysis shows that these cells are intermediate between ISCs and enterocytes (ECs) (Figure 2F). Thus, H15h-C4 cells were identified as EC precursor cells (EPs). The smaller clusters H15h-C5 through H15h-C9 were characterized as differentiated cells (Figure S3B). These differentiated cells are likely the early differentiated progeny of initially labeled *Msi1*<sup>+</sup> cells produced over the 15-h period, suggesting that *Msi1*<sup>+</sup> cells have started the differentiation program.

To understand the hierarchy among distinct cell clusters, we performed pseudo-temporal ordering of scRNA-seq data using Monocle 2, which places cells along putative differentiation trajectories (Qiu et al., 2017). This analysis arranged most ISCs from the H15h-C1, H15h-C2, and H15h-C3 clusters into a major pseudotime trajectory that bifurcates toward ECs and differentiated secretory cells (Figures 2G and S3D). Consistent with cluster identity attribution, ECs are preceded by EPs (H15h-C4 cells) in Path2 of the pseudotime (Figure 2G). A large number of genes were differentially expressed in cells along the pseudotime trajectory (Figure 2H). Among them, a number of “branching” genes were identified, which are potentially important for EC versus secretory cell differentiation (Figure 2I). The scRNA-seq data and its computational analysis suggest that the *Msi1*<sup>CreERT2</sup> allele might mark a heterogeneous population of cells, consisting primarily of ISCs and a small number of differentiated cells and residing along the two major differentiation trajectories.

### Cycling ISCs Initiate Epithelial Regeneration

Next, we sought to define the initial cells that repopulate the epithelium after  $\gamma$ -IR exposure. A minimal number (1–2) of proliferating cells exist in each crypt at 2 days after  $\gamma$ -IR, followed by rapid proliferative expansion between 72–96 h (Figures S4A and S4B). We performed scRNA-seq on the progeny of *Msi1*<sup>+</sup> cells from *Msi1*<sup>CreERT2</sup>;*R26*<sup>mTmG</sup> mice 2 days after  $\gamma$ -IR (refer to IR2), a time point marking the initiation of epithelial regeneration (Kim et al., 2017). Ten distinct cell clusters were identified (Figures 3A, 3B, and S4C–S4E; Table S1). Importantly, the distribution of known ISC marker genes changed dramatically (Figure 3C). Compared to the distribution of *Msi1*<sup>+</sup> cells during homeostasis, the *Lgr5*<sup>high</sup> cell cluster was depleted 2 days after  $\gamma$ -IR (Figure 3C). Consistently, the number of *Lgr5*<sup>high</sup> cells becomes markedly reduced 2 days after  $\gamma$ -IR or treatment with the DNA replication inhibitor and chemotherapeutic agent 5-fluorouracil (5-FU) (De Angelis et al., 2006). In contrast, the number of *Msi1*<sup>+</sup> cells showed an increasing trend, albeit not significant, upon these treatments (Figures 3D and S4F). Cluster

exposure, and harvested 3 days after 12 Gy  $\gamma$ -IR. Scale bar, 10  $\mu$ m. Quantification of LacZ<sup>+</sup> ribbons under the indicated conditions. Data represent the mean value  $\pm$  SD. NS, not significant; \*p < 0.05 (Student's t test).

(H) *Msi1*<sup>CreERT2</sup>;*R26*<sup>sl-DTA</sup> mice irradiated 15 h after TAM induction and then harvested 3 days after  $\gamma$ -IR. Immunohistochemistry for Ki67 under the indicated conditions. Scale bar, 100  $\mu$ m.

(I) Quantification of regenerative foci in (H) (Ctrl, n = 117 crypts, n = 3 mice; DTA, n = 139 crypts, n = 3 mice). Data represent the mean value  $\pm$  SD. \*\*\*p < 0.001 (Student's t test).

See also Figures S1 and S2.

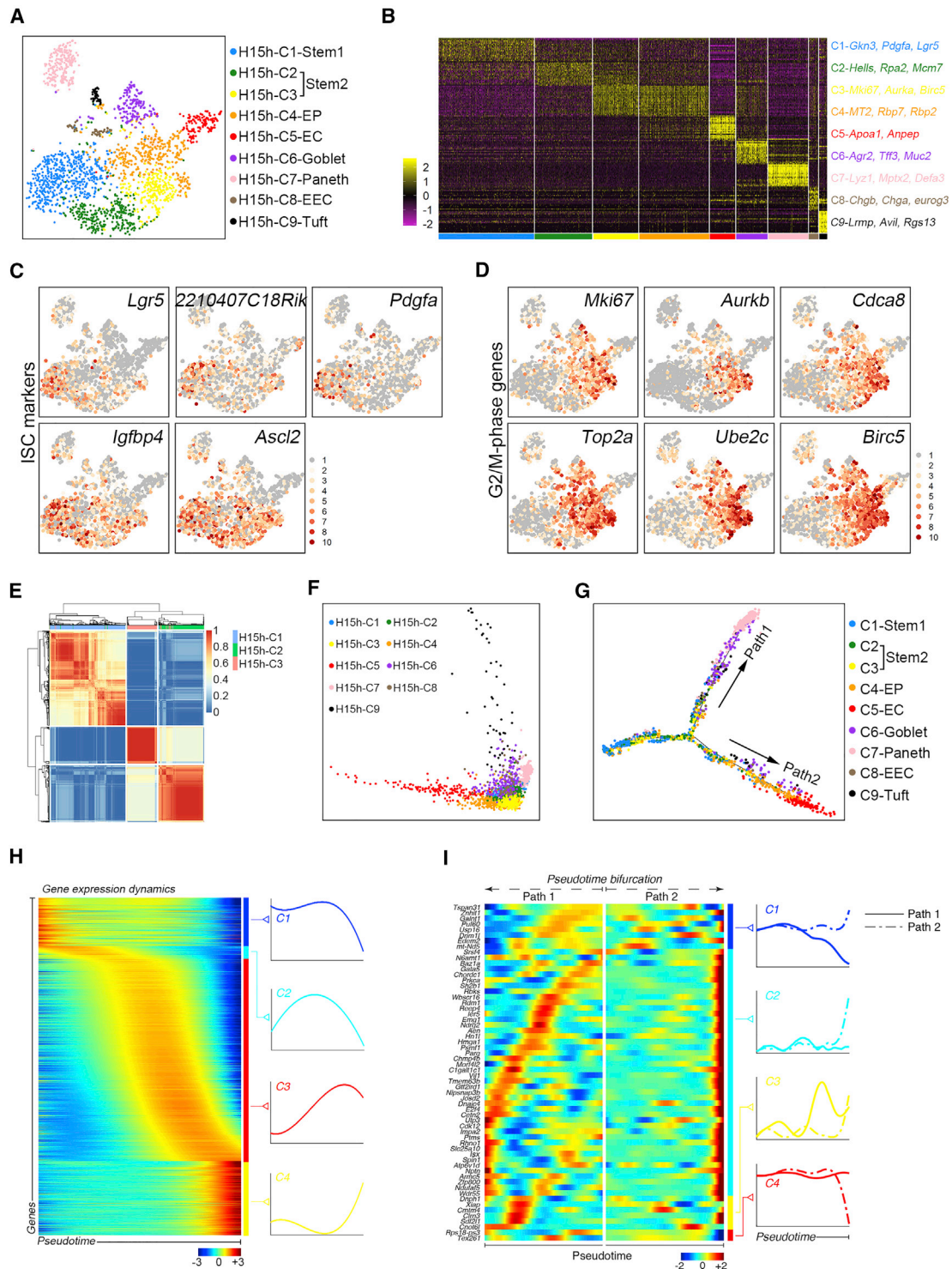


**Figure 2. *Msi1*<sup>+</sup> Cells Are a Heterogeneous Population**

(A) A t-distributed stochastic neighbor embedding (t-SNE) plot revealed cellular heterogeneity of 2329 *Msi1*<sup>+</sup> cells sorted from *Msi1*<sup>CreERT2</sup>; *R26*<sup>mTmG</sup> mice 15 h after TAM induction.

(B) Heatmap of differentially expressed genes in each cluster.

(C and D) Feature plots of expression distribution for ISC (C) and G2/M phase (D) marker genes.

(E) SC3 analysis showing the correlation of H15h-C1 to H15h-C3.

(F) PCA showing the association of distinct cell clusters.

(legend continued on next page)



IR2-C1 cells are identified as ISCs, because they strongly expressed ISC marker genes *Igf1bp4* and *Ascl2* (Figure 3C). IR2-C2 cells were identified as a transition cluster due to their intermediate position between ISCs and differentiated cells (Figure 3E). IR2-C1 and -C2 cells are enriched for genes functioning on DNA damage response (DDR) and cell survival (Figures 3F and S4G), suggesting a strong DDR. In the pseudotime trajectory, IR2-C1 and IR1-C2 cells are enriched at the starting point of the major branch, whereas IR2-C3 and IR2-C4 cells are enriched at the end of EC branch, with the remaining cells enriched at the end of the secretory/differentiated branch (Figure 3G). Consequently, few cells localize around the pseudotime bifurcation as compared with normal physiological conditions (Figure 3G). Given that WNT pathway activation is critical for regeneration of damaged intestinal epithelium after  $\gamma$ -IR. The distribution of WNT downstream target genes *Axin2* and *Ascl2*, as well as surface receptor genes for Wnt ligand, *Lrp5* and *Lrp6* showed that WNT pathway is activated in IR2-C1/C2 stem cells (Figures 3C and 3H). Importantly, IR2-C1 and IR2-C2 cells are cycling, whereas the other cells primarily reside in G0/G1 phase (Figures 3I and S4H; Tables S2 and S3). These data suggest that IR2-C1 and IR2-C2 cells are cycling ISCs that initiate epithelial regeneration.

Previous reports indicated that radioresistant +4 cells are dormant (Montgomery et al., 2011; Powell et al., 2012; Yan et al., 2012). Therefore, on scRNA-seq, we expected to see a certain number of quiescent ISCs (in G0/G1 phase), along with proliferatively active ISCs. In contrast, we found that  $\sim$ 42% of IR2-C1 cells were in S phase, and 58% were in G2/M phase. There were no G0/G1-phase IR2-C1 cells (Figure 3I; Table S2). IR2-C1 cluster also strongly expressed proliferating marker genes (Figure S4H; Table S3). These data suggest that quiescent ISCs are lacking at this stage. Next, we considered that 2 days after  $\gamma$ -IR might be too late to detect surviving quiescent ISCs. Thus, we performed scRNA-seq on the progeny of *Msi1*<sup>+</sup> cells from *Msi1*<sup>CreERT2</sup>; *R26*<sup>mTmG</sup> mice 1 day after  $\gamma$ -IR, a time point when the majority of intestinal cells are undergoing cell death. Two clusters of ISCs were identified (Figures S4I and S4J; Table S1), and surprisingly, they also exhibited a highly proliferative state, with no cells in G0/G1 phase (Figures 3J and S4K; Table S2). Together, these data demonstrate that cycling, rather than quiescent ISCs, initiate epithelial regeneration. It also raises the possibility that a population of cycling ISCs is resistant to and can survive  $\gamma$ -IR exposure.

### Cycling *Msi1*<sup>+</sup> ISCs Survive from Exposure to High Dose of $\gamma$ -IR

To test whether cycling ISCs survive from exposure to high dose of  $\gamma$ -IR, we labeled S-phase *Msi1*<sup>+</sup> cells using a 90 min pulse of 5-ethynyl-2'-deoxyuridine (EdU) at a very low dose of 0.017 mg/25 g body weight, which is insufficient to label all S-phase cells (Figure S5A), and then irradiated the mice. Indeed,

we found that the labeled S-phase *Msi1*<sup>+</sup> cells survived  $\gamma$ -IR and divided, and the EdU signals diluted over time (Figure 4A). We then went back to the homeostatic condition and analyzed cell-cycle phases of cells in intestinal crypts by quantifying the positions of PCNA<sup>+</sup>, EdU<sup>+</sup>, and pH3<sup>+</sup> cells. Most cells in the +1 and +2 positions, which are usually considered to be *Lgr5*<sup>high</sup> CBCs (Barker et al., 2007), were in G1 phase (Figure 4B), whereas the cells from positions 4 to 6, referred to as *Lgr5*<sup>low/neg</sup> +4 cells with DNA damage resistance (Powell et al., 2012; Takeda et al., 2011), were in S or G2/M phases (Figure 4B). We then analyzed the division kinetics using dual bromodeoxyuridine (BrdU)/EdU labeling and revealed that the average length of the cell cycle for +4 cells is 13.28 h (n = 177 crypts from 3 mice), whereas that of CBCs is 18.12 h (n = 249 crypts from 3 mice) (Figure 4C). Furthermore, EdU labeling assay revealed that more *Msi1*<sup>+</sup> cells were in S phase compared to *Lgr5*<sup>high</sup> CBCs (Figures 4D and 4E). Similar findings were also observed in *Hopx* reporter marked cells (Figures 4D and 4E). In agreement with those results, the majority of *Lgr5*<sup>low/neg</sup> ISCs from H15h-C2 and H15h-C3 scRNA-seq clusters reside in S and G2/M phases during homeostasis, whereas the majority of *Lgr5*<sup>high</sup> ISCs reside in G1 phase (Figure 4F; Table S2). It has been shown that the signaling pathways regulating the DDR also activate during normal S phase for genome integrity maintenance (Ben-Yehoyada et al., 2007), and this property can increase cellular resistance to DNA damage. Accordingly, DDR genes are specifically enriched in cycling H15h-C2 cells (Figures 4G and S5B). H15h-C2 and H15h-C3 cells are enriched for genes functioning in cell survival and stress, which might facilitate cell survival after exposure to  $\gamma$ -IR (Figure S5C). The HR-mediated DNA repair only occurs in cycling cells at S and G2 phases, enabling an accurate repair of DNA damage (Maity et al., 1994; Moynahan and Jasin, 2010; Shaltiel et al., 2015). We found that the key components of HR-type repair such as *Rad51*, *Rad51ap1*, *Brca1*, *Brca2*, and *Smc6* are highly expressed in the ISCs populations 1 and 2 days after  $\gamma$ -IR (Figures 4H and S5D), suggesting a strong HR-type repair response in S- and G2-phase ISCs. Taken together, these findings strongly suggest that the DNA damage-resistant *Msi1*<sup>+</sup> cells are more rapidly cycling than *Lgr5*<sup>high</sup> CBCs.

### *Msi1*<sup>+</sup> Cells Repopulate the Intestinal Epithelium at Early Stage When *Lgr5*<sup>high</sup> Cells Are Not Emerging

To define the mechanism underlying *Msi1*<sup>+</sup> ISC-mediated epithelial regeneration, we also performed scRNA-seq on *Msi1*<sup>+</sup> cell progeny 3 and 5 days after  $\gamma$ -IR (refer to IR3 and IR5). Three days after  $\gamma$ -IR, considered as proliferative phase (Kim et al., 2017), ten distinct cell clusters were identified (Figures 5A, 5B, and S6A; Table S1). ISCs are subdivided into two clusters, IR3-C1 and IR3-C2. The first cluster is highly enriched for DDR genes (Figure 5C) and DNA helicases (Figure S6B), and most cells are in S phase (Figure S6C; Table S2). Compared to

(G) Pseudotime ordering on *Msi1*<sup>+</sup> cells.

(H) scEpath analysis performed on pseudotime along the trajectory from stem cells to differentiated cells, identifying four gene clusters (C1–C4) of pseudotime-dependent genes.

(I) scEpath analysis identifying four gene clusters (C1–C4) of branching genes. See also Figure S3 and Table S1.

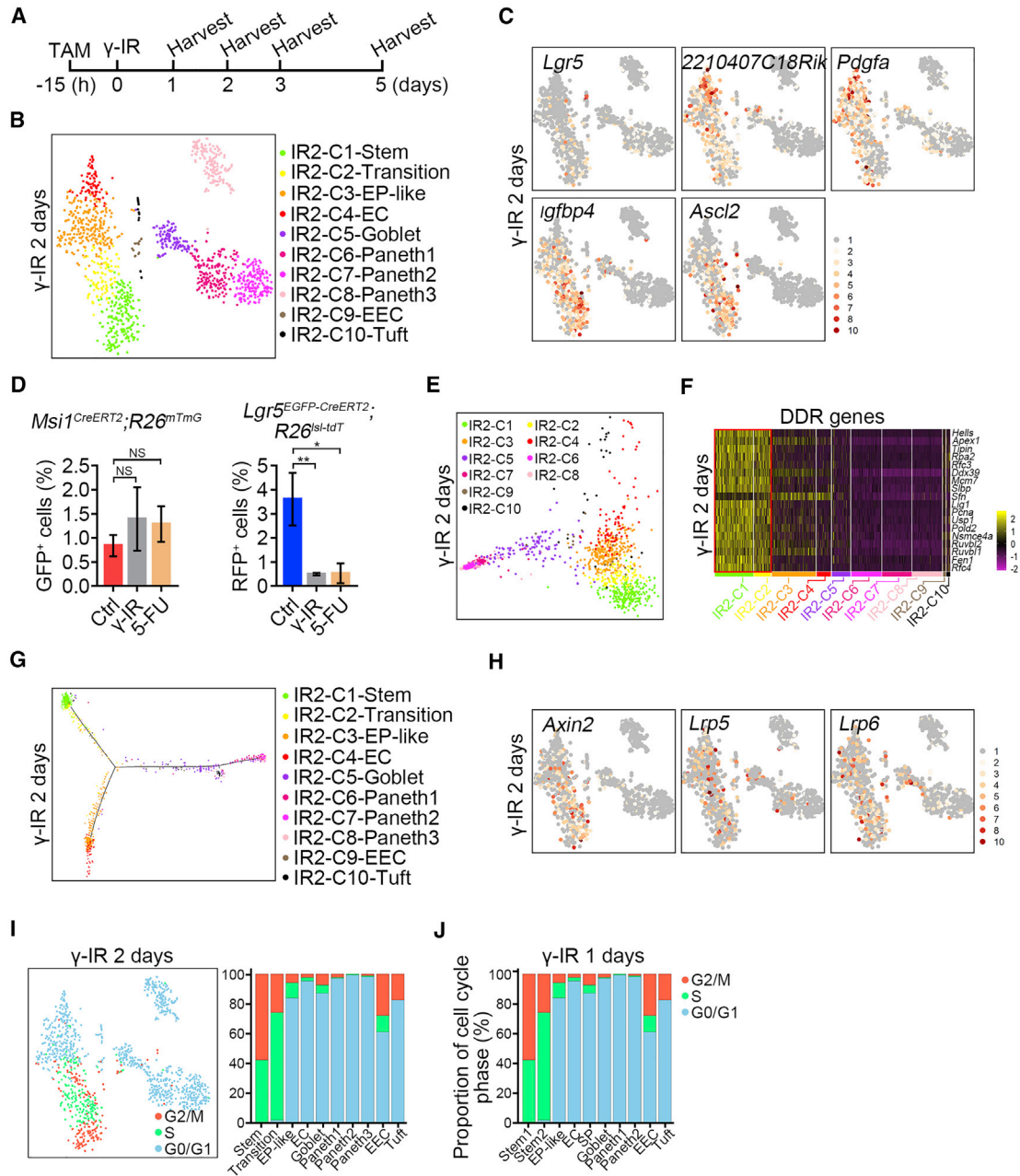


### Figure 3. Cycling ISCs Initiate Intestinal Epithelial Regeneration

(A) Strategy of sample collection for scRNA-seq after  $\gamma$ -IR.

(B) A t-SNE plot revealed cellular heterogeneity of 1,335 *Msi1*<sup>+</sup> cell progeny from *Msi1*<sup>CreERT2</sup>;*R26*<sup>mTmG</sup> mice 2 days after  $\gamma$ -IR. The mice were pretreated with TAM 15 h before  $\gamma$ -IR.

(C) Feature plots of expression distribution for ISC marker genes 2 days after  $\gamma$ -IR.

(D) Quantification of *Msi1*<sup>+</sup> (n = 3 mice) and *Lgr5*<sup>+</sup> (n = 3 mice) populations 2 days after treatment with  $\gamma$ -IR or 5-FU. Mice were treated with  $\gamma$ -IR or two consecutive doses of 5-FU and then induced by TAM 15 h before sacrifice, as shown in Figure S4F. Data represent the mean value  $\pm$  SD. NS, not significant; \*\*p < 0.01 (Student's t test).

(E) PCA showing the association of distinct cell clusters 2 days after  $\gamma$ -IR.

(F) Heatmap of DDR genes in distinct clusters 2 days after  $\gamma$ -IR.

(G) Pseudotime ordering of *Msi1*<sup>+</sup> cell progeny 2 days after  $\gamma$ -IR.

(H) Feature plots of expression distribution for WNT pathway-related genes 2 days after  $\gamma$ -IR.

(I) Cell-cycle metrics of *Msi1*<sup>+</sup> cell progeny 2 days after  $\gamma$ -IR.

(J) Proportions of cell-cycle stages in each cluster 1 day after  $\gamma$ -IR.

See also Figure S4 and Tables S2 and S3.



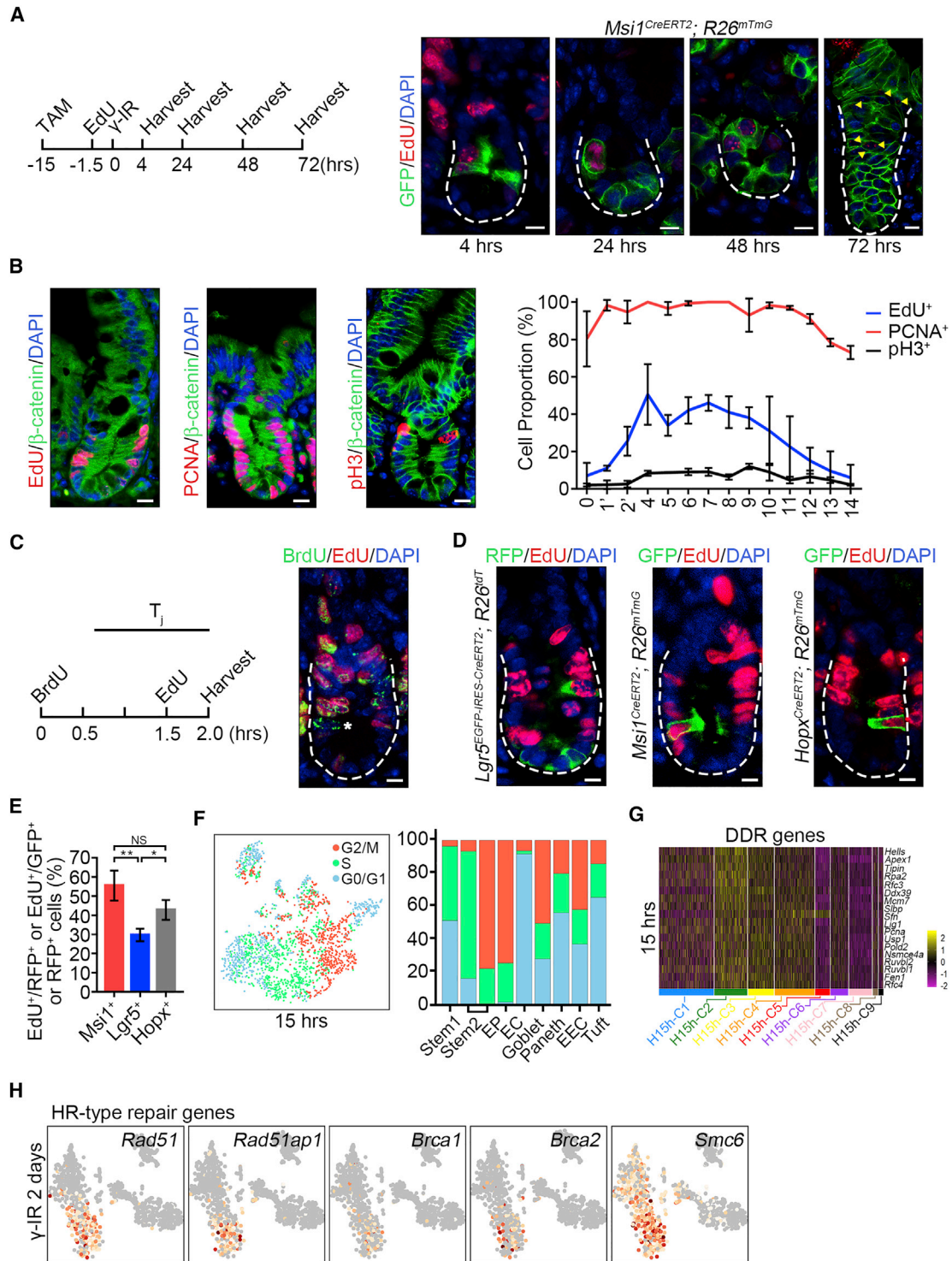


**Figure 4. *Msi1*<sup>+</sup> Cells Are More Rapidly Cycling Compared to CBCs**

(A) Strategy of testing whether EdU-labeled S-phase *Msi1*<sup>+</sup> cells survive from  $\gamma$ -IR exposure. *Msi1<sup>CreERT2</sup>; R26<sup>mTmG</sup>* mice were treated by TAM and labeled using a 90-min pulse of EdU at 0.017 mg/25 g body weight 13.5 h after TAM induction and then irradiated 15 h after TAM induction. Immunofluorescence for EdU and GFP in intestinal crypts at the indicated time points. n = 3 mice at each time point. Scale bar, 10  $\mu$ m.

(B) Immunofluorescence for EdU/ $\beta$ -catenin, PCNA/ $\beta$ -catenin, and phosphor-histone 3/ $\beta$ -catenin in the intestinal crypts of WT mice. Scale bar, 10  $\mu$ m. Quantification of EdU<sup>+</sup> (n = 100 crypts; n = 3 mice), PCNA<sup>+</sup> (n = 59 crypts; n = 3 mice) and pH3<sup>+</sup> (n = 202 crypts; n = 3 mice) cells at the indicated position of intestinal crypts. Data represent the mean value  $\pm$  SD.

(legend continued on next page)

IR3-C1, IR3-C2 cells are characterized by reduced levels of DDR and DNA helicase genes (Figures 5C and S6B) and exhibit increased proliferative capacity, as evidenced by the enrichment for proliferating marker genes (Figure S6D; Table S3). Indeed, over 90% of IR3-C2 cells were in G2/M phase (Figure S6C). IR3-C3 cells localize in the EC branch before EP-like cells (Figure 5D), and most of them were in S and G2/M phases. Thus, IR3-C3 cells were identified as proliferating EPs. In comparison, IR3-C4 cells are dormant EP-like cells and are in G0/G1 phase (Figure S6C). Another important finding is that secretory precursors (SPs, IR3-C6) start to emerge at this stage. The cells are defined by *Dll1* expression (van Es et al., 2012) (Figure S6E), rapid proliferation (Figure S6C), and close relatedness to secretory differentiated cells in the pseudotime trajectory (Figure 5D) and on PCA analysis (Figure S6F). Many proliferating goblet cells were identified 3 days after  $\gamma$ -IR, compared to 2 days (Figures 5B and S6C). Interestingly, *Lgr5<sup>high</sup>* CBCs are not emerging at this stage (Figures 5B and S6G). In agreement, immunohistochemical assay showed that the proportion of *Lgr5<sup>+</sup>* cells is the lowest 3 days after  $\gamma$ -IR (Figures 5E and S6H). Thus, it appears that surviving ISCs directly give rise to proliferating EPs and proliferating SPs at early stage when *Lgr5<sup>high</sup>* cells are not emerging.

Five days after  $\gamma$ -IR, tissue enters the normalization phase (Kim et al., 2017), and dramatic changes were observed at this time in *Msi1<sup>+</sup>* progeny on scRNA-seq (Figures 5F, S6I, and S6J; Table S1). Compared to 3 days after  $\gamma$ -IR, the populations of EC and goblet cells expand dramatically (Figures 5F and 5G; Table S4), whereas EP-like cells almost entirely disappear (Figure 5F). The increase in goblet cells was further confirmed by immunofluorescence (Figures 5H and 5I). Another striking finding was the emergence of a new type of stem cell (IR5-C1), which is very similar to the *Lgr5<sup>high</sup>* ISC population in physiology and is characterized by the enrichment of *Lgr5<sup>+</sup>*, *2210407C18Ric<sup>+</sup>*, and *Pdgrfa<sup>+</sup>* accompanied by the appearance of *Igf1bp4<sup>+</sup>*, *Ascl2<sup>+</sup>*, and *Olfm4<sup>+</sup>* (Figure 5J). Similar to homeostatic *Lgr5<sup>high</sup>* ISCs, a large number of IR5-C1 cells reside in G1 phase (Figures 5K and 5L; Table S2). Furthermore, the RNA velocity (La Manno et al., 2018) on IR5-C1, IR5-C2, and IR5-C3 clusters revealed that IR5-C1 cells are likely derived from IR5-C2 and IR5-C3 cells (Figures 5M and S6K). Together, our data indicate that new IR5-C1 cells are nascent *Lgr5<sup>high</sup>* ISCs. Overall, we posit that during epithelial regeneration, surviving ISCs directly give rise to proliferative precursors of differentiated lineages, and only later do they regenerate relatively slowly cycling *Lgr5<sup>high</sup>* ISCs. We conclude that the *Msi1<sup>+</sup>* cells repopulate the intestinal epithelium at early stage when *Lgr5<sup>high</sup>* cells are not emerging and give rise to nascent *Lgr5<sup>high</sup>* cells only at later time.

### *Msi1<sup>+</sup>* ISCs Preferentially Produce Paneth Cells

Another striking finding that drew our attention was the dynamic change in Paneth cells during epithelial regeneration. Two days after  $\gamma$ -IR, Paneth cells are the most abundant cell type, accounting for 39% (Figures 6A and S4D; Table S4), with this proportion decreasing to  $\sim$ 10% 3–5 days after  $\gamma$ -IR (Figures 6A, S7A, and S7B; Table S4). Lineage-tracing analysis revealed a large number of *Msi1<sup>+</sup>* cell-derived Paneth cells (over 25%) residing in the regenerative unit 2 days after  $\gamma$ -IR (Figures 6B and 6C). Three days after  $\gamma$ -IR, small and large regenerative units existed (Figure 6B). The proportion of *Msi1<sup>+</sup>* cell-derived Paneth cells is much higher in the small regenerative units than in the large ones (Figure 6D). On scRNA-seq, 2 days after  $\gamma$ -IR, Paneth cells can be divided into three distinct clusters based on marker genes (Figure 6E). Compared with type 1 and type 2 Paneth cells, type 3 cells exhibit increased levels of *Gm14851* and *Defa22* and reduced level of *Mptx2*. Expression levels of *AY761184* and *Defa3* appear to gradually increase from Paneth cell type 1 to type 3 (Figure S7C). Type 1 Paneth cells, which were transcriptionally closest to goblet cells, gradually changed to type 2 and finally to type 3 (Figure S4D). This finding suggests a gradual maturation process in the direction of Paneth cell type 1 to type 2 to type 3. We also noticed that Paneth cell markers, such as *Lyz1*, *Defa17*, and *Gm15284* were expanded in the goblet cell population (Figure 6E), whereas they are usually specific for Paneth cells during homeostasis (Figure S3B). At this stage, Paneth cells are preferentially generated relative to goblet cells. Paneth cells have been identified as a niche for ISCs under physiological conditions (Sato et al., 2011). Accordingly, the ISC ligand *Wnt3* was highly enriched in these Paneth cells (Figure 6F). Together, our findings indicate that *Msi1<sup>+</sup>* cells preferentially give rise to Paneth cells upon exposure to  $\gamma$ -IR.

Considering the increase in *Msi1<sup>+</sup>* cell-derived Paneth cells 2 days after  $\gamma$ -IR, we sought to examine whether *Msi1<sup>+</sup>* cells preferentially produce Paneth cells under normal physiological conditions. We quantified the number of Paneth cells after lineage tracing in *Lgr5<sup>EGFP-IRES-CreERT2</sup>;R26<sup>lsI-tD</sup>* and *Msi1<sup>CreERT2</sup>;R26<sup>mTmG</sup>* mice 2 days after TAM induction. Strikingly, we found that the proportion of *Msi1<sup>+</sup>* cell-derived Paneth cells is  $\sim$ 10.76%, whereas *Lgr5<sup>+</sup>* cell-derived Paneth cells are just 0.58% (Figures 6G and 6H). We also observed that the proportion of *Lgr5<sup>+</sup>* cell-derived Paneth cells increased with the lineage tracing time (Figures 6I and S7D), most likely due to the increase of *Msi1<sup>+</sup>* cells derived from *Lgr5<sup>+</sup>* cells with time. The finding of +4 cells preferentially generating Paneth cells was further confirmed by lineage tracing in *Hopx<sup>CreERT2</sup>;R26<sup>mTmG</sup>* mice 2 days after TAM treatment (Figures 6G and 6H). These data

(C) Schematics of the EdU and BrdU temporary space pulse method to calculate the average length of cell-cycle times (left). Cells still in S phase during the labeled time were EdU<sup>+</sup>BrdU<sup>+</sup>, whereas cells that exited S phase were EdU<sup>-</sup>BrdU<sup>+</sup>, indicated by asterisks (right).

(D) Immunofluorescence for RFP and EdU in intestines from *Lgr5<sup>EGFP-CreERT2</sup>;R26<sup>lsI-tD</sup>* mice 15 h after TAM induction, and immunofluorescence for GFP and EdU in intestines from *Msi1<sup>CreERT2</sup>;R26<sup>mTmG</sup>* and *Hopx<sup>CreERT2</sup>;R26<sup>mTmG</sup>* mice 15 h after TAM induction. Scale bar, 10  $\mu$ m.

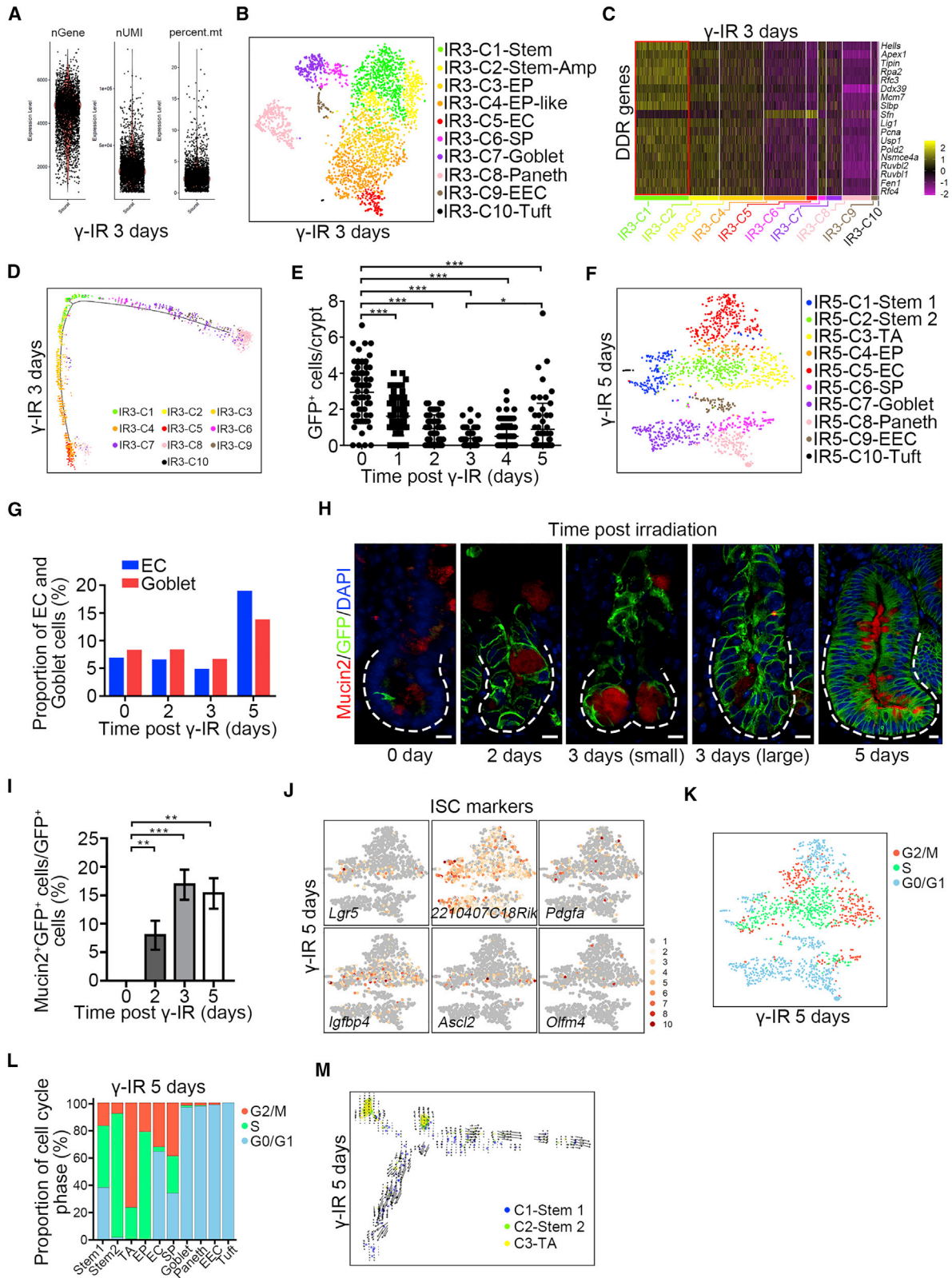
(E) Quantification of RFP<sup>+</sup>/EdU<sup>+</sup> cells in *Lgr5<sup>EGFP-CreERT2</sup>;R26<sup>lsI-tD</sup>* intestinal crypts (n = 268 cells; n = 3 mice) and GFP<sup>+</sup>/EdU<sup>+</sup> cells in *Msi1<sup>CreERT2</sup>;R26<sup>mTmG</sup>* (n = 162 cells; n = 3 mice) and *Hopx<sup>CreERT2</sup>;R26<sup>mTmG</sup>* (n = 200 cells; n = 3 mice) intestinal crypts in (D). Data represent the mean value  $\pm$  SD. NS, not significant; \*p < 0.05; \*\*p < 0.01 (Student's t test).

(F) Cell-cycle metrics of *Msi1<sup>+</sup>* cells at homeostasis.

(G) Heatmap of DDR genes in distinct clusters of *Msi1<sup>+</sup>* cells.

(H) Feature plots of expression distribution for the key genes functioning in HR-type DNA damage repair 2 days after  $\gamma$ -IR.

See also Figure S5.



(legend on next page)



suggest that *Msi1*<sup>+</sup> cells preferentially generate Paneth cells as compared to *Lgr5*<sup>+</sup> cells. To further confirm this idea, we performed scRNA-seq on labeled cells in intestinal crypt from *Lgr5*<sup>EGFP-IRES-CreERT2;R26<sup>sl-tdT</sup></sup> and *Msi1*<sup>CreERT2;R26<sup>mTmG</sup></sup> mice 2 days after TAM induction. Consistently, we also found that the proportion of Paneth cells in *Msi1*<sup>+</sup> cell progeny is much higher than that of the *Lgr5*<sup>+</sup> progeny (Figures 6J and S7E–S7H; Table S4). In comparison, the proportions of goblet, tuft, and EC cells were similar between them (Figure 6J). Collectively, our findings strongly indicate that *Msi1*<sup>+</sup> cells preferentially produce Paneth cells during homeostasis relative to *Lgr5*<sup>+</sup> cells.

## DISCUSSION

Our findings strongly indicate that the DNA damage-resistant subset of *Msi1*<sup>+</sup> ISCs, most likely *Lgr5*<sup>low/neg</sup> ISCs, are more rapidly cycling than *Lgr5*<sup>high</sup> CBCs (Figure 7), rather than quiescent, which substantially differs from the current intestinal stem cell theory. Classically, +4 cells have been identified as quiescent ISCs, whereas *Lgr5*<sup>+</sup> CBCs were thought to be rapidly cycling (Montgomery et al., 2011; Powell et al., 2012; Sangiorgi and Capecchi, 2008; Takeda et al., 2011; Yan et al., 2012). The notion of +4 ISCs dormancy was mainly supported by their colocalization with label-retaining cells in pulse-chase experiments. However, the +4 location of label-retaining cells (Potten et al., 1974, 2002) has been challenged by a number of subsequent studies. Three independent works demonstrated that the long-term label-retaining cells in intestinal crypts were Paneth cells, and short-term label-retaining cells were SPs undergoing commitment toward Paneth and EEC lineages (Buczacki et al., 2013; Li et al., 2016; Steinhauser et al., 2012). Likewise, *Bmi1*-expressing cells were recently identified as EEC lineage cells that possess ISC activity (Yan et al., 2017), although they were considered slow-cycling ISCs resistant to irradiation (Yan et al., 2012). Those conclusions contrast the notion that +4 cells are quiescent label-retaining ISCs. Our findings that +4 cells cycle faster than *Lgr5*<sup>high</sup> cells is further supported by recent work, showing that *Lgr5*<sup>high</sup> CBCs are in an unlicensed G1 phase,

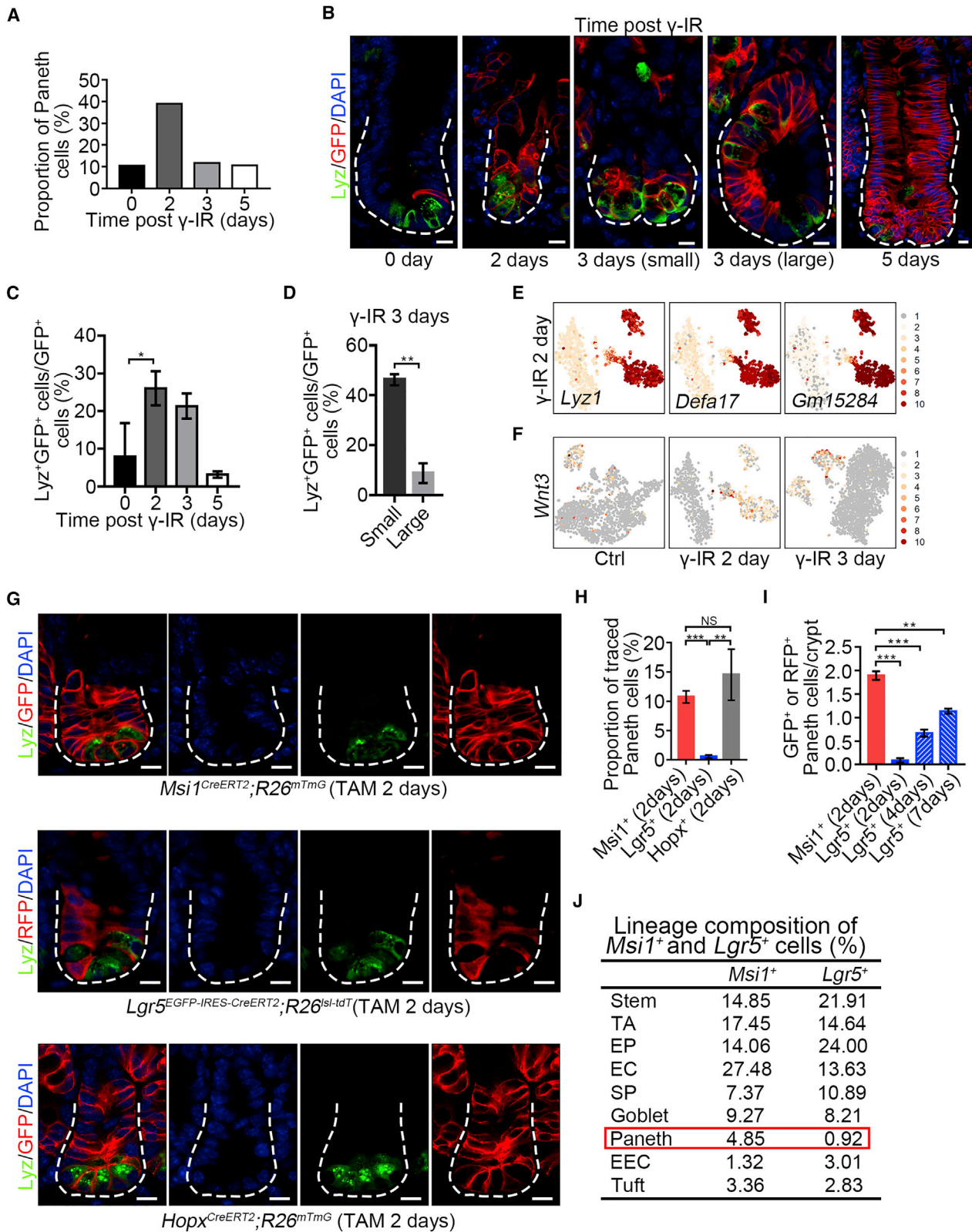
whereas most cells in the +4 to +8 positions are in S phase (Carroll et al., 2018).

Classic +4 ISC theory states that quiescent +4 cells become activated in response to  $\gamma$ -IR. However, to the best of our knowledge, this idea lacks direct evidence. In contrast, it is well established that following  $\gamma$ -IR exposure, cells either transiently block cell-cycle progression to allow time for DNA repair, or exist cell cycle permanently (Shaltiel et al., 2015). G1 arrest, S-phase delay, or G2 arrest can all take place following  $\gamma$ -IR-induced damage. Importantly, G1 arrest typically occurs at lower doses of  $\gamma$ -IR, whereas S-phase delay and G2 arrest are common at higher doses to allow for cells to repair DNA damage (Maity et al., 1994). Accordingly, HR-mediated DNA repair, which enables an accurate repair using the sister chromatid as the template, can only occur in cycling cells during late S and G2 phases to repair DNA damage, making the cells survive from  $\gamma$ -IR exposure (Moynahan and Jasin, 2010). Another important factor in rendering S-phase cells resistant to DNA damage is that the signaling pathways regulating response to acute DNA damage also operate during normal S phase to maintain genome integrity in the presence of low levels of replication-associated damage (Ben-Yehoyada et al., 2007). Indeed, S-phase cells have been shown to be the least sensitive to  $\gamma$ -IR (Pawlik and Keyomarsi, 2004). Consistently, we found that DNA damage repair genes are enriched in a subset of *Msi1*<sup>+</sup> cells during S and G2/M phases. Thus, we posit that the *Msi1*<sup>+</sup> ISCs during S and G2/M phase possess the capacity to resist DNA damage.

Although our data indicate that it is the cycling *Msi1*<sup>+</sup> ISCs that survive  $\gamma$ -IR exposure and repopulate damaged epithelium, we cannot formally rule out the previously proposed model that quiescent ISCs and/or precursors also contribute to epithelial regeneration (Ayyaz et al., 2019; Chaves-Pérez et al., 2019; Yan et al., 2017). It is noteworthy that, although many secretory progenitor cells, marked by *Dll1*<sup>CreERT</sup> (van Es et al., 2012), *Prox1*<sup>CreERT</sup> (Yan et al., 2017), or H2B-label (Buczacki et al., 2013), have regenerative capacity, the contribution of these cells to epithelial regeneration are limited (Bankaitis et al., 2018). In comparison, the cycling *Msi1*<sup>+</sup> ISCs might

### Figure 5. *Msi1*<sup>+</sup> Cells Repopulate the Intestinal Epithelium at Early Stage When *Lgr5*<sup>high</sup> Cells Are Not Emerging

- (A) scRNA-seq data quality control of *Msi1*<sup>+</sup> cell progeny from *Msi1*<sup>CreERT2;R26<sup>mTmG</sup></sup> mice 3 days after  $\gamma$ -IR. The mice were pretreated with tamoxifen 15 h before  $\gamma$ -IR.
- (B) A t-SNE plot revealed cellular heterogeneity of 3124 *Msi1*<sup>+</sup> cell progeny from *Msi1*<sup>CreERT2;R26<sup>mTmG</sup></sup> mice 3 days after  $\gamma$ -IR.
- (C) Heatmap of DDR genes in distinct clusters 3 days after  $\gamma$ -IR.
- (D) Pseudotime ordering on *Msi1*<sup>+</sup> cell progeny 3 days after  $\gamma$ -IR.
- (E) Quantification of GFP<sup>+</sup> cells in the intestinal crypts of *Lgr5*<sup>EGFP-IRES-CreERT2</sup> mice at the indicated time points after  $\gamma$ -IR. 180 intestinal crypts (60 crypts/mouse, n = 3 mice) were quantified at each time point. Representative images were shown in Figure S6H. Data represent the mean value  $\pm$  SD. \*p < 0.05; \*\*\*p < 0.001 (Student's t test).
- (F) A t-SNE plot revealed cellular heterogeneity of 1,556 *Msi1*<sup>+</sup> cell progeny from *Msi1*<sup>CreERT2;R26<sup>mTmG</sup></sup> mice 5 days after  $\gamma$ -IR.
- (G) The proportion of EC and goblet populations of scRNA-seq results at the indicated time points after  $\gamma$ -IR.
- (H) Immunofluorescence for Mucin2 and GFP in *Msi1*<sup>CreERT2;R26<sup>mTmG</sup></sup> normal intestinal crypts and regenerative foci at the indicated time points after  $\gamma$ -IR. "small" indicates small regenerative foci; "large" indicates large regenerative foci. Scale bar, 10  $\mu$ m.
- (I) Quantification of the percentage of Mucin2<sup>+</sup>GFP<sup>+</sup> cells versus GFP<sup>+</sup> cells (n = 365 crypts, n = 3 mice per chase time point) in (H). Data represent the mean value  $\pm$  SD. \*\*p < 0.01, \*\*\*p < 0.001 (Student's t test).
- (J) Feature plots of expression distribution for ISC marker genes 5 days after  $\gamma$ -IR.
- (K) Cell-cycle metrics on *Msi1*<sup>+</sup> cell progeny 5 days after  $\gamma$ -IR.
- (L) Proportions of cell-cycle stages in each cluster 5 days after  $\gamma$ -IR.
- (M) RNA velocity analysis of IR5-C1 to IR5-C3 across the pseudotime trajectory 5 days after  $\gamma$ -IR.
- See also Figure S6 and Table S4.



(legend on next page)

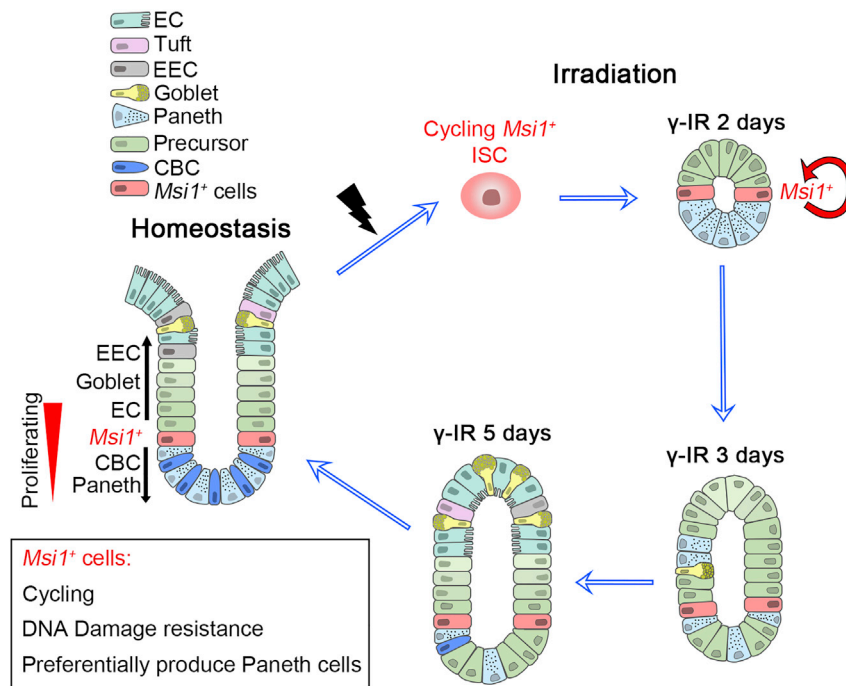


**Figure 7. A Model of *Msi1*<sup>+</sup> Cells in Maintaining and Regenerating Intestinal Epithelium**

A subset of *Msi1*<sup>+</sup> ISC that exhibit DNA-damage resistance are cycling faster than *Lgr5*<sup>high</sup> CBCs, and fast repopulation of the intestinal epithelium at early stage when *Lgr5*<sup>high</sup> cells are not emerging. *Msi1*<sup>+</sup> cells preferentially produce Paneth cells during homeostasis and upon radiation repair.

quick repopulation of the damaged intestinal epithelium with a high efficiency. Thus, the two types of cells are apparently different, both at homeostasis and damage regeneration. Furthermore, it is worth mentioning that the primary DNA damage repair pathway in quiescent stem cells in other tissues such as hematopoietic system—NHEJ—is error-prone, resulting in genome instability due to the accumulation of subtle mutations and chromosomal aberrations (Mohrin et al., 2010). If quiescent ISCs also use the same mechanism, many DNA mutations and chromosomal aberrations would exist in the surviving quiescent ISCs

represent a primary source for regenerating intestinal epithelium. The quiescent LRCs can also generate Paneth cells and participate in the regeneration of damaged intestinal epithelium (Buczacki et al., 2013), but they are significantly different from *Msi1*<sup>+</sup> ISCs. First, the majority of quiescent LRCs were secretory progenitors and committed to differentiated secretory cells mostly within a week (Buczacki et al., 2013). In comparison, the *Msi1* reporter<sup>+</sup> cells were cycling stem cells that can contribute the whole lineage of intestinal epithelium, and *Msi1* reporter-marked progeny existed for at least 1 year. Second, only a few clones were traced by the initial labeled LRCs 2 weeks after damage (Buczacki et al., 2013), suggesting a low efficiency of regeneration. In comparison, *Msi1* reporter<sup>+</sup> cells enable a

after  $\gamma$ -IR exposure. This would be detrimental to normal epithelial regeneration and would contribute to tumorigenesis. Therefore, we believe that cycling ISCs survive  $\gamma$ -IR exposure due to the high-fidelity HR-type repair.

Our data also demonstrate that the surviving *Msi1*<sup>+</sup> cells repopulate damaged intestinal epithelium at early stage when *Lgr5*<sup>high</sup> cells are not emerging and give rise to nascent *Lgr5*<sup>high</sup> cells only at later time. This observation substantially differs from the prevailing idea that dormant surviving +4 cells function as reserve stem cells that, upon activation, generate rapidly cycling *Lgr5*<sup>high</sup> cells that then go on to produce all differentiated lineages (Li and Clevers, 2010). Indeed, in our lineage studies, progeny of *Msi1*<sup>+</sup> cells can initially move

**Figure 6. *Msi1*<sup>+</sup> ISCs Preferentially Generate Paneth Cells 2 Days after  $\gamma$ -IR**

- (A) The proportion of Paneth cells in scRNA-seq results at indicated time points after  $\gamma$ -IR.  
 (B) Immunofluorescence for lysozyme and GFP in normal intestinal crypts and regenerative foci from *Msi1*<sup>CreERT2</sup>;*R26*<sup>mTmG</sup> mice at indicated time points after  $\gamma$ -IR. “small” indicates small regenerative foci; “large” indicated large regenerative foci. Scale bar, 10  $\mu$ m.  
 (C) Quantification of Lyz<sup>+</sup>/GFP<sup>+</sup> versus GFP<sup>+</sup> cells at indicated time points in (B) (n = 562 crypts, n = 3 mice per chase time point). Data represent the mean value  $\pm$  SD. \*p < 0.05 (Student’s t test).  
 (D) Quantification of Lyz<sup>+</sup>/GFP<sup>+</sup> versus GFP<sup>+</sup> cells in small (n = 133 crypts; n = 3 mice) and large (n = 66 crypts; n = 3 mice) regenerative foci 3 days after  $\gamma$ -IR. Data represent the mean value  $\pm$  SD. \*\*p < 0.01 (Student’s t test).  
 (E) Feature plots of expression distribution for Paneth cell marker genes 2 days after  $\gamma$ -IR.  
 (F) Feature plots of *wnt3* distribution at indicated time points after  $\gamma$ -IR.  
 (G) Immunofluorescence for lysozyme and GFP/RFP in intestinal crypts from *Msi1*<sup>CreERT2</sup>;*R26*<sup>mTmG</sup>, *Lgr5*<sup>EGFP-CreERT2</sup>;*R26*<sup>sl-tdT</sup>, and *Hopx*<sup>CreERT2</sup>;*R26*<sup>mTmG</sup> mice 2 days after TAM induction. Scale bar, 10  $\mu$ m.  
 (H) Quantification of Lyz<sup>+</sup>/GFP<sup>+</sup> versus GFP<sup>+</sup> or Lyz<sup>+</sup>/RFP<sup>+</sup> versus RFP<sup>+</sup> cells in (G) (n = 365 crypts, n = 3 mice per chase time point). Data represent the mean value  $\pm$  SD. \*\*p < 0.01; \*\*\*p < 0.001; NS, not significant (Student’s t test).  
 (I) Quantification of the number of GFP<sup>+</sup> or RFP<sup>+</sup> Paneth cells in each crypt from *Msi1*<sup>CreERT2</sup>;*R26*<sup>mTmG</sup> and *Lgr5*<sup>EGFP-CreERT2</sup>;*R26*<sup>sl-tdT</sup> mice at indicated time points after TAM induction (n = 409 crypts, n = 3 mice per chase time point). Representative images are shown in Figure S7D. Data represent the mean value  $\pm$  SD. \*\*p < 0.01; \*\*\*p < 0.001 (Student’s t test).  
 (J) scRNA sequencing revealed lineage composition of *Msi1*<sup>CreERT2</sup>;*R26*<sup>mTmG</sup> and *Lgr5*<sup>EGFP-CreERT2</sup>;*R26*<sup>sl-tdT</sup> mice 2 days after TAM induction. The t-SNE plots are shown in Figures S7G and S7H.  
 See also Figure S7.



both up and down the crypt relative to +4 positions in normal physiology, suggesting that they generate their progeny independent of *Lgr5<sup>high</sup>* CBCs during homeostasis. In agreement with our observation, classic cell migration tracing studies also demonstrated that all crypt cells ultimately derive from cells located at approximately the +4 position (Kaur and Potten, 1986; Potten, 1998; Qiu et al., 1994). In other words, *Lgr5<sup>high</sup>* ISCs are not the only direct progeny of +4 ISCs. Thus, we posit that a subset of *Msi1<sup>+</sup>* cells might be bona fide ISCs responsible for both normal homeostasis and epithelial regeneration (Figure 7).

## STAR★METHODS

Detailed methods are provided in the online version of this paper and include the following:

- KEY RESOURCES TABLE
- RESOURCE AVAILABILITY
  - Lead Contact
  - Materials Availability
  - Data and Code Availability
- EXPERIMENTAL MODEL AND SUBJECT DETAILS
- METHOD DETAILS
  - Lineage tracing
  - LacZ staining
  - Dual-staining for EdU and BrdU
  - Histology, Immunohistochemistry (IHC) and Immunofluorescence (IF) assays
  - Cell cycle calculation
  - *In situ* hybridization
  - Flow cytometry
  - Intestinal organoids culture
  - qRT-PCR analysis
  - Single-cell mRNA sequencing
  - Primary computational analysis
  - Pseudotime
  - Identification of pseudotime-dependent gene dynamics
- QUANTIFICATION AND STATISTICAL ANALYSIS

## SUPPLEMENTAL INFORMATION

Supplemental Information can be found online at <https://doi.org/10.1016/j.celrep.2020.107952>.

## ACKNOWLEDGMENTS

Z.Y. is funded by grants from the National Natural Science Foundation of China (81772984 and 81572614); the Major Project for Cultivation Technology (2016ZX08008001 and 2014ZX08008001); Basic Research Program (2015QC0104, 2015TC041, 2016SY001, 2016QC086, 2019TC227, and 2019TC088); and an SKLB Open Grant (2020SKLAB6-18). C.F.G.-J. is supported by the University of California, Irvine Chancellor's ADVANCE Postdoctoral Fellowship Program. Z. Lin. is supported by NIH T32-Training Program in Cancer Biology and Therapeutics. B.A. is supported by RO1AR44882.

## AUTHOR CONTRIBUTIONS

Z.Y. and F.R. designed research. X.S., C.L., C.S., X.B., M.D., J.X., M.L., X.W., Q.W., X.Y., G.L., and R.Z. performed research. X.S., Z. Lin, C.F.G.-J., X.L.,

Q.N., W.C., S.G., H.Z., Z. Liu, Y.C., M.V.P., C.J.L., B.A., F.R., and Z.Y. analyzed data. X.S., C.L., and Z.Y. wrote the manuscript.

## DECLARATION OF INTERESTS

The authors declare no competing interests.

Received: June 25, 2019

Revised: January 9, 2020

Accepted: July 2, 2020

Published: July 28, 2020

## REFERENCES

- Ayyaz, A., Kumar, S., Sangiorgi, B., Ghoshal, B., Gosio, J., Ouladan, S., Fink, M., Barutcu, S., Trcka, D., Shen, J., et al. (2019). Single-cell transcriptomes of the regenerating intestine reveal a revival stem cell. *Nature* 569, 121–125.
- Bankaitis, E.D., Ha, A., Kuo, C.J., and Magness, S.T. (2018). Reserve Stem Cells in Intestinal Homeostasis and Injury. *Gastroenterology* 155, 1348–1361.
- Barker, N. (2014). Adult intestinal stem cells: critical drivers of epithelial homeostasis and regeneration. *Nat. Rev. Mol. Cell Biol.* 15, 19–33.
- Barker, N., van Es, J.H., Kuipers, J., Kujala, P., van den Born, M., Cozijnsen, M., Haegebarth, A., Korving, J., Begthel, H., Peters, P.J., and Clevers, H. (2007). Identification of stem cells in small intestine and colon by marker gene *Lgr5*. *Nature* 449, 1003–1007.
- Ben-Yehoyada, M., Gautier, J., and Dupré, A. (2007). The DNA damage response during an unperturbed S-phase. *DNA Repair (Amst.)* 6, 914–922.
- Buczacki, S.J., Zecchini, H.I., Nicholson, A.M., Russell, R., Vermeulen, L., Kemp, R., and Winton, D.J. (2013). Intestinal label-retaining cells are secretory precursors expressing *Lgr5*. *Nature* 495, 65–69.
- Butler, A., Hoffman, P., Smibert, P., Papalexi, E., and Satija, R. (2018). Integrating single-cell transcriptomic data across different conditions, technologies, and species. *Nat. Biotechnol.* 36, 411–420.
- Carroll, T.D., Newton, I.P., Chen, Y., Blow, J.J., and Näthke, I. (2018). *Lgr5<sup>+</sup>* intestinal stem cells reside in an unlicensed G<sub>1</sub> phase. *J. Cell Biol.* 217, 1667–1685.
- Chaves-Pérez, A., Yilmaz, M., Perna, C., de la Rosa, S., and Djouder, N. (2019). URI is required to maintain intestinal architecture during ionizing radiation. *Science* 364, eaaq1165.
- De Angelis, P.M., Svendsrud, D.H., Kravik, K.L., and Stokke, T. (2006). Cellular response to 5-fluorouracil (5-FU) in 5-FU-resistant colon cancer cell lines during treatment and recovery. *Mol. Cancer* 5, 20.
- Duò, A., Robinson, M.D., and Sonesson, C. (2018). A systematic performance evaluation of clustering methods for single-cell RNA-seq data. *F1000Res.* 7, 1141.
- Gehart, H., and Clevers, H. (2015). Repairing organs: lessons from intestine and liver. *Trends Genet.* 31, 344–351.
- Guerrero-Juarez, C.F., Dedhia, P.H., Jin, S., Ruiz-Vega, R., Ma, D., Liu, Y., Yamaga, K., Shestova, O., Gay, D.L., Yang, Z., et al. (2019). Single-cell analysis reveals fibroblast heterogeneity and myeloid-derived adipocyte progenitors in murine skin wounds. *Nat. Commun.* 10, 650.
- Heath, J.P. (1996). Epithelial cell migration in the intestine. *Cell Biol. Int.* 20, 139–146.
- Jin, S., MacLean, A.L., Peng, T., and Nie, Q. (2018). scEpath: energy landscape-based inference of transition probabilities and cellular trajectories from single-cell transcriptomic data. *Bioinformatics* 34, 2077–2086.
- Jones, K.B., Furukawa, S., Marangoni, P., Ma, H., Pinkard, H., D'Urso, R., Zilionis, R., Klein, A.M., and Klein, O.D. (2019). Quantitative Clonal Analysis and Single-Cell Transcriptomics Reveal Division Kinetics, Hierarchy, and Fate of Oral Epithelial Progenitor Cells. *Cell Stem Cell* 24, 183–192.
- Kaur, P., and Potten, C.S. (1986). Circadian variation in migration velocity in small intestinal epithelium. *Cell Tissue Kinet.* 19, 591–599.

- Kayahara, T., Sawada, M., Takaishi, S., Fukui, H., Seno, H., Fukuzawa, H., Suzuki, K., Hiai, H., Kageyama, R., Okano, H., and Chiba, T. (2003). Candidate markers for stem and early progenitor cells, Musashi-1 and Hes1, are expressed in crypt base columnar cells of mouse small intestine. *FEBS Lett.* **535**, 131–135.
- Kim, C.K., Yang, V.W., and Bialkowska, A.B. (2017). The Role of Intestinal Stem Cells in Epithelial Regeneration Following Radiation-Induced Gut Injury. *Curr. Stem Cell Rep.* **3**, 320–332.
- Kiselev, V.Y., Kirschner, K., Schaub, M.T., Andrews, T., Yiu, A., Chandra, T., Natarajan, K.N., Reik, W., Barahona, M., Green, A.R., and Hemberg, M. (2017). SC3: consensus clustering of single-cell RNA-seq data. *Nat. Methods* **14**, 483–486.
- Kowalczyk, M.S., Tirosh, I., Heckl, D., Rao, T.N., Dixit, A., Haas, B.J., Schneider, R.K., Wagers, A.J., Ebert, B.L., and Regev, A. (2015). Single-cell RNA-seq reveals changes in cell cycle and differentiation programs upon aging of hematopoietic stem cells. *Genome Res.* **25**, 1860–1872.
- La Manno, G., Soldatov, R., Zeisel, A., Braun, E., Hochgerner, H., Petukhov, V., Lidschreiber, K., Kastrioti, M.E., Lönnerberg, P., Furlan, A., et al. (2018). RNA velocity of single cells. *Nature* **560**, 494–498.
- Li, L., and Clevers, H. (2010). Coexistence of quiescent and active adult stem cells in mammals. *Science* **327**, 542–545.
- Li, N., Yousefi, M., Nakauka-Ddamba, A., Jain, R., Tobias, J., Epstein, J.A., Jensen, S.T., and Lengner, C.J. (2014). Single-cell analysis of proxy reporter allele-marked epithelial cells establishes intestinal stem cell hierarchy. *Stem Cell Reports* **3**, 876–891.
- Li, N., Yousefi, M., Nakauka-Ddamba, A., Li, F., Vandivier, L., Parada, K., Woo, D.H., Wang, S., Naqvi, A.S., Rao, S., et al. (2015). The Msi Family of RNA-Binding Proteins Function Redundantly as Intestinal Oncoproteins. *Cell Rep.* **13**, 2440–2455.
- Li, N., Nakauka-Ddamba, A., Tobias, J., Jensen, S.T., and Lengner, C.J. (2016). Mouse Label-Retaining Cells Are Molecularly and Functionally Distinct From Reserve Intestinal Stem Cells. *Gastroenterology* **151**, 298–310.
- Maity, A., McKenna, W.G., and Muschel, R.J. (1994). The molecular basis for cell cycle delays following ionizing radiation: a review. *Radiother. Oncol.* **31**, 1–13.
- McDavid, A., Finak, G., Chattopadhyay, P.K., Dominguez, M., Lamoreaux, L., Ma, S.S., Roederer, M., and Gottardo, R. (2013). Data exploration, quality control and testing in single-cell qPCR-based gene expression experiments. *Bioinformatics* **29**, 461–467.
- Metcalfe, C., Kijavín, N.M., Ybarra, R., and de Sauvage, F.J. (2014). Lgr5+ stem cells are indispensable for radiation-induced intestinal regeneration. *Cell Stem Cell* **14**, 149–159.
- Mohrin, M., Bourke, E., Alexander, D., Warr, M.R., Barry-Holson, K., Le Beau, M.M., Morrison, C.G., and Passequé, E. (2010). Hematopoietic stem cell quiescence promotes error-prone DNA repair and mutagenesis. *Cell Stem Cell* **7**, 174–185.
- Montgomery, R.K., Carlone, D.L., Richmond, C.A., Farilla, L., Kranendonk, M.E., Henderson, D.E., Baffour-Awuah, N.Y., Ambruzs, D.M., Fogli, L.K., Algra, S., and Breault, D.T. (2011). Mouse telomerase reverse transcriptase (mTert) expression marks slowly cycling intestinal stem cells. *Proc. Natl. Acad. Sci. USA* **108**, 179–184.
- Moynahan, M.E., and Jasin, M. (2010). Mitotic homologous recombination maintains genomic stability and suppresses tumorigenesis. *Nat. Rev. Mol. Cell Biol.* **11**, 196–207.
- Pawlik, T.M., and Keyomarsi, K. (2004). Role of cell cycle in mediating sensitivity to radiotherapy. *Int. J. Radiat. Oncol. Biol. Phys.* **59**, 928–942.
- Potten, C.S. (1998). Stem cells in gastrointestinal epithelium: numbers, characteristics and death. *Philos. Trans. R. Soc. Lond. B Biol. Sci.* **353**, 821–830.
- Potten, C.S., Kovacs, L., and Hamilton, E. (1974). Continuous labelling studies on mouse skin and intestine. *Cell Tissue Kinet.* **7**, 271–283.
- Potten, C.S., Owen, G., and Booth, D. (2002). Intestinal stem cells protect their genome by selective segregation of template DNA strands. *J. Cell Sci.* **115**, 2381–2388.
- Powell, A.E., Wang, Y., Li, Y., Poulin, E.J., Means, A.L., Washington, M.K., Higinbotham, J.N., Juchheim, A., Prasad, N., Levy, S.E., et al. (2012). The pan-ErbB negative regulator Lrig1 is an intestinal stem cell marker that functions as a tumor suppressor. *Cell* **149**, 146–158.
- Qiu, J.M., Roberts, S.A., and Potten, C.S. (1994). Cell migration in the small and large bowel shows a strong circadian rhythm. *Epithelial Cell Biol.* **3**, 137–148.
- Qiu, X., Hill, A., Packer, J., Lin, D., Ma, Y.A., and Trapnell, C. (2017). Single-cell mRNA quantification and differential analysis with Census. *Nat. Methods* **14**, 309–315.
- Sangiorgi, E., and Capecchi, M.R. (2008). Bmi1 is expressed in vivo in intestinal stem cells. *Nat. Genet.* **40**, 915–920.
- Sato, T., Vries, R.G., Snippert, H.J., van de Wetering, M., Barker, N., Stange, D.E., van Es, J.H., Abo, A., Kujala, P., Peters, P.J., and Clevers, H. (2009). Single Lgr5 stem cells build crypt-villus structures in vitro without a mesenchymal niche. *Nature* **459**, 262–265.
- Sato, T., van Es, J.H., Snippert, H.J., Stange, D.E., Vries, R.G., van den Born, M., Barker, N., Shroyer, N.F., van de Wetering, M., and Clevers, H. (2011). Paneth cells constitute the niche for Lgr5 stem cells in intestinal crypts. *Nature* **469**, 415–418.
- Shaltiel, I.A., Krenning, L., Bruinsma, W., and Medema, R.H. (2015). The same, only different - DNA damage checkpoints and their reversal throughout the cell cycle. *J. Cell Sci.* **128**, 607–620.
- Shibui, S., Hoshino, T., Vanderlaan, M., and Gray, J.W. (1989). Double labeling with iodo- and bromodeoxyuridine for cell kinetics studies. *J. Histochem. Cytochem.* **37**, 1007–1011.
- Stacey, R., and Green, J.T. (2014). Radiation-induced small bowel disease: latest developments and clinical guidance. *Ther. Adv. Chronic Dis.* **5**, 15–29.
- Steinhauser, M.L., Bailey, A.P., Senyo, S.E., Guillemier, C., Perlstein, T.S., Gould, A.P., Lee, R.T., and Lechene, C.P. (2012). Multi-isotope imaging mass spectrometry quantifies stem cell division and metabolism. *Nature* **481**, 516–519.
- Takeda, N., Jain, R., LeBoeuf, M.R., Wang, Q., Lu, M.M., and Epstein, J.A. (2011). Interconversion between intestinal stem cell populations in distinct niches. *Science* **334**, 1420–1424.
- Tetteh, P.W., Basak, O., Farin, H.F., Wiebrands, K., Kretschmar, K., Begthel, H., van den Born, M., Korving, J., de Sauvage, F., van Es, J.H., et al. (2016). Replacement of Lost Lgr5-Positive Stem Cells through Plasticity of Their Enterocyte-Lineage Daughters. *Cell Stem Cell* **18**, 203–213.
- Tian, H., Biehs, B., Warming, S., Leong, K.G., Rangell, L., Klein, O.D., and de Sauvage, F.J. (2011). A reserve stem cell population in small intestine renders Lgr5-positive cells dispensable. *Nature* **478**, 255–259.
- van Es, J.H., Sato, T., van de Wetering, M., Lyubimova, A., Yee Nee, A.N., Gregorieff, A., Sasaki, N., Zeinstra, L., van den Born, M., Korving, J., et al. (2012). Dll1+ secretory progenitor cells revert to stem cells upon crypt damage. *Nat. Cell Biol.* **14**, 1099–1104.
- Yan, K.S., Chia, L.A., Li, X., Ootani, A., Su, J., Lee, J.Y., Su, N., Luo, Y., Heilshorn, S.C., Amieva, M.R., et al. (2012). The intestinal stem cell markers Bmi1 and Lgr5 identify two functionally distinct populations. *Proc. Natl. Acad. Sci. USA* **109**, 466–471.
- Yan, K.S., Gevaert, O., Zheng, G.X.Y., Anchang, B., Probert, C.S., Larkin, K.A., Davies, P.S., Cheng, Z.F., Kaddis, J.S., Han, A., et al. (2017). Intestinal Enterendocrine Lineage Cells Possess Homeostatic and Injury-Inducible Stem Cell Activity. *Cell Stem Cell* **21**, 78–90.
- Yu, S., Tong, K., Zhao, Y., Balasubramanian, I., Yap, G.S., Ferraris, R.P., Bonder, E.M., Verzi, M.P., and Gao, N. (2018). Paneth Cell Multipotency Induced by Notch Activation following Injury. *Cell Stem Cell* **23**, 46–59.

STAR★METHODS

KEY RESOURCES TABLE

REAGENT or RESOURCE	SOURCE	IDENTIFIER
<b>Antibodies</b>		
Rat anti-BrdU	Abcam	Cat# ab6326; RRID: AB_305426
Rabbit anti-Ki67	Thermo Fisher	Cat# RM-9106-S1; RRID: AB_149792
Rabbit anti-Cleaved Caspase-3	Cell Signaling Technology	Cat# 9664S; RRID: AB_2070042
Goat anti-Lysozyme C	Santa Cruz	Cat# sc-27958; RRID: AB_2138790
Rabbit anti-Chromogranin A	Abcam	Cat# ab15160; RRID: AB_301704
Rabbit anti-Mucin2	Santa Cruz	Cat# sc-15334; RRID: AB_2146667
Mouse anti-Histone H3, phospho (Ser10)	Abcam	Cat# ab14955; RRID: AB_443110
Rabbit anti-PCNA	Abcam	Cat# ab92552; RRID: AB_10561973
Rat anti-Msi1	MBL	Cat# D270-3; RRID: AB_1953023
Chicken anti-GFP	Abcam	Cat# ab13970; RRID: AB_300798
Rabbit anti-GFP	Abcam	Cat# ab290; RRID: AB_303395
Rabbit anti-RFP	ROCKLAND	Cat# 600-401-379; RRID: AB_2209751
Rat anti-CD45	eBioscience	Cat# 17-0451-82; RRID: AB_469392
Rat anti-CD31	eBioscience	Cat# 17-0311-82; RRID: AB_657735
Rat anti-TER 119	eBioscience	Cat# 17-5921-82; RRID: AB_469473
<b>Chemicals, Peptides, and Recombinant Proteins</b>		
Tamoxifen (TAM)	Sigma-Aldrich	Cat# T5648
5-fluorouracil (5-FU)	Sigma-Aldrich	Cat# F6627
Diphtheria Toxin (DT)	Sigma-Aldrich	Cat# D0564
5-ethynyl-20-deoxyuridine (EdU)	Thermo Fisher	Cat# A10044
Ethylene glycol-bis(2-aminoethylether)- <i>N,N,N',N'</i> -tetraacetic acid (EGTA)	Sigma-Aldrich	Cat# E4378
5-bromo-20-deoxyuridine (BrdU)	Sigma-Aldrich	Cat# B5002
Ethylenedinitrilotetraacetic acid (EDTA)	Sigma-Aldrich	Cat# E9884
Dispase	Stem Cell Technologies	Cat# 07913
Fixable Viability Dye	eBioscience	Cat# 65-0863-14
IntestiCult™ Organoid Growth Medium (Mouse)	Stem Cell Technologies	Cat# 06005
4-hydroxytamoxifen (4-OH)	Sigma-Aldrich	Cat# H6278
TRIZol	Invitrogen	Cat# 10296010
LightCycler 480 SYBR Green I master mix	Roche	Cat# 04887352001
Matrigel	Corning	Cat# 356231
<b>Critical Commercial Assays</b>		
Click-iT EdU Alexa Flour 594 Kit	Beyotime	Cat# C0078S
Advanced Cell Diagnostics RNAscope 2.5 HD detection Reagents-RED kit	ACD	Cat# 322360
RNeasy Plus Mini Kit	QIAGEN	Cat# 74134
Single cell 3 'Library and Gel Bead Kit V2	10x Genomics	Cat# 120237
Chromium Single Cell A Chip Kit	10x Genomics	Cat# 120236
<b>Deposited Data</b>		
Single-cell RNA sequencing data	This paper	GEO: GSE145866
<b>Experimental Models: Organisms/Strains</b>		
Mouse: <i>Msi1<sup>CreERT2</sup></i>	This paper	N/A
Mouse: <i>Lgr5<sup>EGFP-IRES-CreERT2</sup></i>	The Jackson Laboratory	JAX# 008875
Mouse: <i>R26<sup>tmG</sup></i>	The Jackson Laboratory	JAX# 007676

(Continued on next page)



**Continued**

REAGENT or RESOURCE	SOURCE	IDENTIFIER
Mouse: $R26^{tdT}$	The Jackson Laboratory	JAX# 007914
Mouse: $R26R^{LacZ}$	The Jackson Laboratory	JAX# 009427
Mouse: $R26^{Isl-DTA}$	The Jackson Laboratory	JAX# 010527
Mouse: $R26^{Isl-DTR}$	The Jackson Laboratory	JAX# 007900
Mouse: $Hopx^{CreERT2}$	The Jackson Laboratory	JAX# 017606
Oligonucleotides		
ISH <i>Msi1</i> probe	ACD	Cat# 469801
Genotyping primer, $Msi1^{CreERT2}$ -forward: TGGTTTCGGCCACAGTCTTG	This paper	N/A
Genotyping primer, $Msi1^{CreERT2}$ -resersw: TCCAGCTCGACCAGGATGGG-3	This paper	N/A
Software and Algorithms		
GraphPad Prism 7	GraphPad	N/A
Cellranger 2.0.1	10X Genomics	<a href="https://support.10xgenomics.com/single-cell-gene-expression/software/downloads/latest">https://support.10xgenomics.com/single-cell-gene-expression/software/downloads/latest</a>
Seurat 2.3.4	Butler et al., 2018	<a href="https://satijalab.org/seurat">https://satijalab.org/seurat</a>
Monocle 2.10.1	Qiu et al., 2017	<a href="http://cole-trapnell-lab.github.io/monocle-release/">http://cole-trapnell-lab.github.io/monocle-release/</a>
scEpath	Jin et al., 2018	<a href="https://github.com/sqjin/scEpath">https://github.com/sqjin/scEpath</a>
SC3	Kiselev et al., 2017	<a href="https://www.bioconductor.org/packages/release/bioc/html/SC3.html">https://www.bioconductor.org/packages/release/bioc/html/SC3.html</a>
Velocyto.R	La Manno et al., 2018	<a href="https://github.com/velocyto-team/velocyto.R">https://github.com/velocyto-team/velocyto.R</a>

**RESOURCE AVAILABILITY**

**Lead Contact**

Further information and requests for resources and reagents should be directed to and will be fulfilled by the Lead Contact, Zhengquan Yu ([zyu@cau.edu.cn](mailto:zyu@cau.edu.cn)).

**Materials Availability**

Mouse lines generated in this study are available upon request to Lead Contact provided the requestor covers shipping costs.

**Data and Code Availability**

All scRNA-seq data from this study are available at NCBI Gene Expression Omnibus (GEO). The accession number for data reported in this paper is GEO: GSE145866.

**EXPERIMENTAL MODEL AND SUBJECT DETAILS**

All mouse experiment procedures and protocols were evaluated and authorized by the Regulations of Beijing Laboratory Animal Management and were strictly in accordance with the guidelines of the Institutional Animal Care and Use Committee of China Agricultural University (approval number: SKLAB-2015-04-03).  $Msi1^{CreERT2}$  mice were generated at the Model Animal Research Center of Nanjing University.  $Lgr5^{EGFP-IRES-CreERT2}$ ,  $R26^{mTmG}$ ,  $R26^{tdT}$  and  $R26R^{LacZ}$  mice were purchased from Jackson Laboratories (stock number: 008875, 007676, 007914, 009427).  $Hopx^{CreERT2}$  mice were obtained from John Epstein's laboratory at the University of Pennsylvania.  $R26^{Isl-DTA}$  mice were obtained from Sen Wu's laboratory at China Agricultural University.  $R26^{Isl-DTR}$  mice were obtained from Hua Zhang's laboratory at China Agricultural University. To evaluate the identity of  $Msi1^+$  cells,  $Msi1^{CreERT2}$  mice were crossed with the mouse models listed above and the detailed description were shown in the figure legends and method details. Male and female age-matched mice between 8-10 weeks were utilized for all experiments.

**METHOD DETAILS**

**Lineage tracing**

For lineage tracing, eight-week-old mice were injected with a single pulse of tamoxifen (4 mg/25 g body weight, Sigma-Aldrich, T5648). To label the  $Msi1^+$  cells at homeostasis,  $Msi1^{CreERT2};R26^{mTmG}$  mice were administered with tamoxifen for fifteen hours before sacrifice. For the injury study,  $Msi1^{CreERT2};R26R^{LacZ}$  and  $Lgr5^{EGFP-IRES-CreERT2};R26R^{LacZ}$  mice were treated with 12 Gy  $\gamma$ -IR fifteen

hours after a single pulse of tamoxifen, and sacrificed at indicated time points. In order to examine the survival after high doses of irradiation or cytotoxic damage, *Msi1<sup>CreERT2</sup>;R26<sup>mTmG</sup>*, and *Lgr5<sup>EGFP-IRES-CreERT2</sup>;R26<sup>sl-tdT</sup>* mice were injected intraperitoneally with two doses of 5-FU (100 mg/Kg body weight, Sigma-Aldrich, F6627) within two days or 12 Gy  $\gamma$ -IR once and analyzed with FACS after two days. To exam the influence with the absence of *Msi1<sup>+</sup>* cells during regeneration, *Msi1<sup>CreERT2</sup>;R26<sup>mTmG</sup>;R26<sup>sl-DTR</sup>* mice model were treated with TAM every other day, and four consecutive DT induction (50  $\mu$ g/Kg body weight, Sigma-Aldrich, D0564). Twenty four hours after the last DT injection, *Msi1<sup>CreERT2</sup>;R26<sup>mTmG</sup>* and *Msi1<sup>CreERT2</sup>;R26<sup>mTmG</sup>;R26<sup>sl-DTR</sup>* mice were exposed to 12 Gy  $\gamma$ -IR and analyzed three days after irradiation. For cell proliferation assay, *Msi1<sup>CreERT2</sup>;R26<sup>mTmG</sup>* and *Lgr5<sup>EGFP-IRES-CreERT2</sup>;R26<sup>sl-tdT</sup>* mice were intraperitoneally injected with EdU (0.2 mg/25 g body weight, Thermo Fisher, A10044) for 1.5 hours before sacrifice.

To test whether S-phase *Msi1<sup>+</sup>* cells survived from exposure of 12Gy  $\gamma$ -IR, *Msi1<sup>CreERT2</sup>;R26<sup>mTmG</sup>* were pretreated with tamoxifen, intraperitoneally injected with EdU (0.017 mg/25 g body weight) 13.5 hours after tamoxifen induction, and then exposed to 12 Gy  $\gamma$ -IR 1.5 hours after EdU injection. The intestinal samples were harvested four hours, one day, two days and three days after exposure to  $\gamma$ -IR.

### LacZ staining

Tissues were fixed in fixative solution (0.2% glutaraldehyde, 5 mM EGTA, 2 mM MgCl<sub>2</sub> in PBS) for two hours on ice, rinsed for ten minutes with detergent rinsing solution (0.02% NP40, 0.01% sodium deoxycholate, 2 mM MgCl<sub>2</sub> in PBS) for three times and immersed in X-gal staining solution (5 mM K<sub>3</sub>Fe(CN)<sub>6</sub>, 5 mM K<sub>4</sub>Fe(CN)<sub>6</sub>, 0.02% NP40, 0.01% sodium deoxycholate, 2 mM MgCl<sub>2</sub> 1 mg/mL X-gal in PBS) overnight at 37°C. The stained tissues were fixed in 4% paraformaldehyde (PFA) and dehydrated for paraffin embedding.

### Dual-staining for EdU and BrdU

Five-micrometer tissue paraffin sections were dewaxed, hydrated, incubated in 1 M hydrochloric acid at 37°C for twenty minutes, washed with PBS for three times and antigen retrieval was performed in 10 mM citric acid. The sections were then stained according to the manufacturer's instructions using the Click-iT EdU Alexa Flour 594 kit (Beyotime, C0078S). After staining, the sections were incubated with blocking solution (Beyotime, P0102) for one hour at room temperature and incubated with primary antibody against BrdU (Abcam, ab6326, 1:100) overnight at 37°C. The sections were washed for three times, and incubated with 488-conjugated secondary antibodies (Thermo Fisher, A11006, 1:400) for one hour at room temperature, stained with DAPI for eight minutes, and finally mounted with anti-fluorescence quenching sealing medium.

### Histology, Immunohistochemistry (IHC) and Immunofluorescence (IF) assays

For histological staining, paraffin-embedded and 5- $\mu$ m sections were stained with hematoxylin and eosin (H&E). Periodic acid-Schiff (PAS) staining was performed using standard methods. For immunohistochemistry staining, the sections were deparaffinized with xylene followed by treatment with serial dilutions of ethanol. Antigen-retrieval was performed by heating slides to 95°C for 10 min in 0.01 M citrate buffer (pH 6) in a microwave oven. After cooling to room temperature, sections were incubated with blocking solution for 1 hour after administration of 3% H<sub>2</sub>O<sub>2</sub> to eliminate endogenous peroxidase activity. Then, the sections were incubated with primary antibody overnight at 4°C. The sections were then immunostained by the ABC peroxidase method (Vector Laboratories) with diaminobenzidine as the enzyme substrate and hematoxylin as a counterstain. For immunofluorescence staining, paraffin sections were microwave pretreated in 0.01 M citrate buffer (pH 6.0), and incubated with primary antibodies, then incubated with secondary antibodies (invitrogen) and counterstained with DAPI in mounting media. The primary antibodies included Ki67 (thermo fisher, RM-9106-S1,1:500), cleaved caspase-3 (CST, 9664s, 1:1000), lysozyme C (Santa Cruz, sc-27958, 1:500), ChgA (Abcam, ab15160, 1:400), Mucin2 (Santa Cruz, sc-15334, 1:500), pH3 (Abcam, ab14955, 1:200), BrdU (Abcam, ab6326, 1:100), PCNA (Abcam, ab92552, 1:200), Msi1 (MBL, D270-3, 1:1000), GFP (Abcam, ab13970, 1:800), GFP (Abcam, ab290, 1:800), RFP (ROCKLAND, 600-401-379,1:200).

### Cell cycle calculation

Ten-week-old mice were intraperitoneally injected with EdU (0.2 mg/25 g body weight) 1.5 hours after a pulse of BrdU (1 mg/25 g body weight, Sigma-Aldrich, B5002) and sacrificed 0.5 hours later. The calculation was based on the assumption that EdU and BrdU could not be detected within thirty minutes after administration into mice. The number of cells still in S phase during the labeled time were EdU<sup>+</sup>BrdU<sup>+</sup> (*S*<sub>cells</sub>) whereas cells that had exited S phase were BrdU<sup>+</sup> (*L*<sub>cells</sub>). The average cell cycle time (*T*<sub>c</sub>) and S phase length (*T*<sub>s</sub>) of +4 cells and CBCs were calculated according to the formulas below. The number of proliferating cells (*P*<sub>cells</sub>) was calculated based on the percentage of PCNA<sup>+</sup> cells in each stem cell in Figure 4B. *T*<sub>j</sub> is the time during which cells can labeled with BrdU but not EdU (Jones et al., 2019; Shibui et al., 1989).

$$T_s = T_j \left( \frac{S_{cell}}{L_{cell}} \right); \cdot T_c = T_s \left( \frac{P_{cell}}{S_{cell}} \right)$$

### In situ hybridization

The small intestine of 10-week-old mice was harvested and fixed in neutral buffered formalin (NBF) at room temperature (RT) for twenty four hours before paraffin embedding. The tissues were chopped into 5  $\mu$ m sections and handled using Advanced Cell Diagnostics RNAscope 2.5 HD detection Reagents-RED kit (ACD) with mouse *Msi1* probe (ACD, 469801). The detailed operation steps of *in situ* hybridization were followed according to the manufacturer's instructions (322360-USM).

### Flow cytometry

The single-cell suspension of intestinal epithelium was collected as described previously (Sato et al., 2009). The fresh mouse intestine was cut open longitudinally and the villi were scraped off. The tissue was chopped into 5 mm pieces and incubated with 10 mM EDTA in PBS for thirty minutes at 4°C. The crypt fractions were collected by pipetting and filtered through a 70  $\mu$ m cell strainer (BD biosciences). The gathered crypts were centrifuged at 1200 rpm for five minutes and digested with dispase (1 U/ml, Stem Cell Technologies). The single cell suspension was passed through a 40 $\mu$ m cell strainer (BD biosciences) and stained with Fixable Viability Dye (eBioscience, 65-0863-14) to remove dead cells. The flow cytometry analysis was performed on a BD FACS Arial 3.0. *Msi1*<sup>+</sup> cells were quantified by cells separated from *Msi1*<sup>CreERT2</sup>; *R26*<sup>mTmG</sup> mice 15 hours after tamoxifen induction. *Lgr5*<sup>high</sup> cells were sorted by flow cytometry from *Lgr5*<sup>EGFP-IRES-CreERT2</sup> mice.

### Intestinal organoids culture

The isolation of intestinal crypts was described above. The gathered crypts were washed twice with PBS and collected by centrifuged at 800 rpm for five minutes. The supernatant was removed and the crypts were resuspended into Matrigel (Corning, 356231) and Medium (STEMCELL Technologies, 06005) (1:1 ratio) and plated into 48 well plates. The medium was replaced every other day. To label the initial *Msi1*<sup>+</sup> cells *in vitro*, the intestinal organoids of *Msi1*<sup>CreERT2</sup>; *R26*<sup>mTmG</sup> and *Lgr5*<sup>EGFP-IRES-CreERT2</sup>; *R26*<sup>sl-tdT</sup> mice were cultured and induced with 4-OH (1  $\mu$ M, Sigma-Aldrich, H6278) for 9.5 hours and then replaced with 4-OH-free medium. To test the contribution of *Msi1*<sup>+</sup> cells to regeneration, the organoids were exposed with 6 Gy  $\gamma$ -IR immediately after *Msi1*<sup>+</sup> cells were labeled.

### qRT-PCR analysis

All collected cells were sorted into TRIzol (Invitrogen, 10296010) immediately and total RNA was extracted using the RNeasy Plus Mini Kit (QIAGEN, 74134). Real-time PCR was performed on a LightCycler 480 real-time PCR system (Roche) combined with the LightCycler 480 SYBR Green I master mix (Roche, 04887352001). The primers used for the gene expression assessment were as follows:

*Olfm4*-forward, 5'-CAGCCACTTTCCAATTTCACTG-3'; *Olfm4*-reverse, 5'-GCTGGACATACTCCTTCACCTTA-3';  
*Lgr5*-forward, 5'-CCTACTCGAAGACTTACCCAGT-3'; *Lgr5*-reverse, 5'-GCATTGGGGTGAATGATAGCA-3';  
*Axin2*-forward, 5'-TGACTCTCCTTCCAGATCCCA-3'; *Axin2*-reverse, 5'-TGCCCACACTAGGCTGACA-3';  
*Sox9*-forward, 5'-GCAGACCAGTACCCGCATCT-3'; *Sox9*-reverse, 5'-CGCTTGTCCGTTCTTACC-3';

### Single-cell mRNA sequencing

A single-cell suspension of intestinal epithelium was prepared as described above. The cells were stained with Fixable Viability Dye (eBioscience, 65-0863-14), CD45 (eBioscience, 17-0451-82), CD31 (eBioscience, 17-0311-82), TER119 (eBioscience, 17-5921-82), to remove dead and lin<sup>-</sup> cells, and GFP<sup>+</sup> cells were sorted into EP tubes in single-cell mode by FACS. The collected cells were held on ice before loaded for GemCode single cell platform (10X). Chromium Single Cell 3' v2 libraries were sequenced with a Novaseq 6000 sequencer, with the following sequencing parameters: read 1, 150 cycles; i7 index, 8 cycles and read 2, 150 cycles.

### Primary computational analysis

Raw Illumina data were demultiplexed and processed using Cell Ranger (10X Genomics version Cell Ranger 2.0.1). The MM10 reference transcriptome provided by 10X genomics was used for mapping. Seurat version 2.3.4 was used for filtering and subsequent clustering (Butler et al., 2018). In order to remove partial cells and doublets, cells with less than 1000 genes or more than 7000 genes were removed. Additionally, cells with more than 10% of mitochondrial unique molecular identifiers (UMIs) were removed, as a high proportion of mitochondrial expression in cells is indicative of cell stress/damage during isolation. In order to reduce gene expression noise, genes that are expressed in 6 cells or less are removed. Gene-cell matrices were normalized and scaled in Seurat using default parameters for UMIs. Highly variable genes were found using a lower x threshold of 0.0125 and a y threshold of 0.5. Principal Component Analysis (PCA) was performed using the highly variable genes identified. T-distributed stochastic neighbor embedding (t-SNE) was performed using the PCA reduction. PCA reduction was also used to clusters with standard modularity function. Because of their low numbers, tuft cells in each time point were manually identified based on expression of canonical markers. A likelihood-ratio test for single cell gene expression was used to identify marker genes for each population (McDavid et al., 2013). Single-cell consensus clustering (SC3) analysis was used to validate the robustness of some clusters (Kiselev et al., 2017). Cell cycle analysis was carried out in Seurat using a list of cell cycle genes from the Regev laboratory (Kowalczyk et al., 2015).

### Pseudotime

Monocle version 2.10.1 was used on cells filtered from Seurat to infer differentiation trajectories (Qiu et al., 2017). An expression threshold of 0.1 was applied. The highly variable genes identified from Seurat were used as the ordering filter. DDRTree was used for dimension reduction. Initially, no root state was specified and the cells were ordered in an unsupervised manner. After the trajectory was obtained, a root state was specified based on where the stem cell populations are for subsequent systematic identification of pseudotime-dependent genes.

### Identification of pseudotime-dependent gene dynamics

We performed scEpath (Jin et al., 2018) on Monocle-ordered cells to identify pseudotime-dependent gene expression changes as before (Guerrero-Juarez et al., 2019). Briefly, we compared the standard deviation of the observed gene expressions by randomly permuting the cell order ( $nboot = 100$  permutations). Genes with a standard deviation greater than 0.5 and a Bonferroni-corrected  $p$ -value below a significance level  $\alpha = 0.01$  were considered to be pseudotime-dependent. Pseudotime-dependent mouse transcription factors were annotated using the Animal Transcription Factor Database (AnimalTFDB 2.0).

### QUANTIFICATION AND STATISTICAL ANALYSIS

All statistical analyses were performed using GraphPad Prism 7 software. All data are shown as mean value  $\pm$  SD. Unpaired two-tailed Student's  $t$  test and two-way ANOVA analysis were performed for statistical analyses (\* $p < 0.05$ , \*\* $p < 0.01$ , \*\*\* $p < 0.001$ ).